# Microbe-vegetation-nutrient interactions are associated with long-term carbon accumulation in a northern peatland

Daniel N. Schillereff[1], Jenny K. Sjöström[2], Richard C. Chiverrell[3]

[1]Department of Geography, King's College London

[2]CRETUS Research Centre, Universidade de Santiago de Compostela

[3]School of Environmental Sciences, University of Liverpool

## Abstract:

Northern peatlands are a globally significant carbon store. This reflects the long-term imbalance between productivity and slow decomposition under waterlogged, nutrient-poor conditions. However, the effects of nutrient deposition on carbon cycling remain poorly understood, especially the role of phosphorus and how nutrient input interacts with vegetation and microbes. This study addressed this uncertainty by reconstructing multi-node carbon cycle dynamics over the past 2000 years at Store Mosse, southern Sweden. We integrated measurements of carbon and nutrients, organic compounds and 16S sequencing of microbial communities with palaeovegetation data. We found evidence of strong stratigraphic associations between nodes, with most periods of higher carbon accumulation characterised by higher microbial diversity, *Gammaproteobacteria,* phosphorus content and less recalcitrant organic matter alongside a shift away from *Sphagnum*-dominated peat. Our findings emphasise the importance of studying multiple interacting nodes to more fully understand the drivers of past and future carbon sequestration.

## Introduction

Northern peatlands store approximately one-third of all the Earth's soil carbon (400 - 500 Pg; (Loisel et al., 2017, 2014). This arises from the long-term imbalance between aboveground primary production and slow rates of decomposition within the peat matrix (Gorham, 1991; Moore et al., 2007; Rydin and Jeglum, 2013). Such inefficient breakdown of organic matter reflects the anaerobic, nutrient-poor conditions typical of mid- and high-latitude peatland ecosystems. Carbon burial does not progress steadily through time. Rather, carbon is rapidly released from fresh plant litter within the surface, active layer (acrotelm) then decomposition slows abruptly in the waterlogged, deeper catotelm (Clymo, 1984; Gorham, 1991). Over timescales spanning millennia, northern peatlands show five-fold differences between the slowest and most rapid rates of carbon accumulation (Anderson, 2002;

Beilman et al., 2009; Charman et al., 2013; Gorham et al., 2012; Kylander et al., 2018; Larsson et al., 2017; Malmer and Wallén, 2004; Ratcliffe et al., 2018; Sjöström et al., 2020). Long-term carbon accumulation rates are typically in the order of 5 – 35 g $m^{-2}$ $y^{-1}$ (Loisel et al., 2014).

Multiple factors govern bog carbon accumulation. The hydrological conditions govern the water table depth, which determines the thickness of the aerobic acrotelm relative to the anaerobic catotelm (Belyea and Malmer, 2004; Liu et al., 2022, p. 202; Moore et al., 2007). Temperature can influence primary productivity (Charman et al., 2013), evapotranspiration rates (Roulet et al., 1993) and microbial mineralisation efficiency (Keller et al., 2006; Preston et al., 2012), while plant composition affects decomposition rates through differing recalcitrant properties. Temperate peatlands are often dominated by *Sphagnum* mosses, which have remarkable abilities to thrive in – and potentially promote - anoxic, low-nutrient conditions. *Sphagnum* plants have a refractory internal structure (Scheffer et al., 2001) and contain biochemical compounds (e.g., phenolics) which can inhibit microbial breakdown (Bragazza et al., 2006; van Breemen, 1995; Wang et al., 2015). Phenolic substances build up in peatlands because the anaerobic conditions limit phenol oxidase activity (Tveit et al., 2013). Should a change in environmental conditions enable vascular plants to become established on a bog, more labile litter and shifts in nutrient cycling, microbial dynamics and, in turn, carbon burial, is likely (Malmer et al., 2003). Low nutrient availability is a hallmark of ombrotrophic peatlands, which receive input purely from atmospheric deposition (Aerts et al., 1992; Bragazza et al., 2004; Moore et al., 2019). Plant productivity and microbial activity is limited in in particular by nitrogen (N) and phosphorus (P) availability (Čapek et al., 2018). Shifts in N or P input is therefore a key control on carbon mineralisation by altering either productivity or microbial activity or both (Basiliko et al., 2006; Čapek et al., 2018; Keller et al., 2006; Schillereff et al., 2021).

The dynamics of microbial communities during long-term bog development remain poorly understood. Behaviour in the near-surface, oxygenated acrotelm has been explored in several studies (Jaatinen et al., 2007; Pankratov et al., 2011; Potter et al., 2017; Roth et al., 2023) and microbial communities are known to be vertically stratified (Andersen et al., 2013; Birnbaum et al., 2023; Wang et al., 2024), but fine variability with depth is rarely investigated. Rather, such studies tend to sub-sample at coarse intervals. For example, Wang et al. (2019) and Birnbaum et al. (2023) focused on 10-20, 30-40 and 60-70-cm depths. Tsitko et al. (2014) sub-sampled every 50 centimetres along a seven-metre core. Other studies extracted surface plus one or two deep samples (Concheri et al., 2017; Morales et al., 2006; Preston et al., 2012; Richy et al., 2024; Wang et al., 2024). These sampling resolutions likely mask fine interplay between microbial composition and other nodes of the carbon cycle.

Very few studies have compared deep microbial profiles with a full set of physical and chemical peat properties. A handful of higher-resolution studies show an association between microbial community distributions and nutrient content (Aksenov et al., 2021; Jiang et al., 2021; Lin et al., 2014a, 2014b). Field experiments have explored microbe-nutrient-vegetation interactions (e.g., Basiliko et al., 2006) but it remains unclear whether long-term (decades, centuries, millennia) is well-captured. Equally, multi-proxy palaeoenvironmental studies of Holocene carbon cycling do not incorporate microbial genomics (e.g., Charman et al., 2013).

We concluded in earlier work (Schillereff et al., 2021) that the paucity of high-resolution microbial genomic data from northern peatlands is a significant barrier to understanding the effects of long-term nutrient deposition on carbon burial efficiency. This feeds into wider concerns that the trajectory of the peatland carbon sink under climate change and anthropogenic pressures such as amplified nutrient deposition remains unclear (Goldstein et al., 2020; Loisel and Gallego-Sala, 2022).

To tackle this uncertainty, we reconstructed multiple nodes of the carbon cycle over the last 2000 years at Store Mosse, southern Sweden. We directly measured carbon and nutrient dynamics and organic matter quality, conducted 16S sequencing of the microbial communites and coupled these data with local vegetation and regional hydroclimate reconstructions. We focus on the last 2000 years, a crucial period of natural and anthropogenic environmental change (PAGES2k, 2017). We find evidence of tight interplay between microbial communities, nutrients and vegetation, which in turn is associated with variation in the carbon accumulation rate at intervals of a few decades to centuries.

## Study site

The pristine portion of the large Store Mosse wetland complex (~77 km$^2$) in south-central Sweden (57°17'54 N, 14°00'39 E) is an ideal study site (Figure 1). Store Mosse has a long history of peat extraction before becoming a protected National Park in 1982. Today, it is haven for birdlife, extensive peat restoration is underway (van Ravenhorst, 2022) and there are many active field experiments (e.g., Robroek et al., 2024). Store Mosse is also a pioneering site for palaeoenvironmental research. Previous studies have demonstrated that Store Mosse box complex developed from a lake to a fen (c. 9000 cal yr BP), followed by ombrotrophic conditions from around 6000-5600 cal yr BP, depending location (Svensson 1988; Kylander et a. 2013; Ryberg et al. 2022; Martínez Cortizas et al., 2021). During the ombrotrophic stage, shifts in wetness, fires, vegetation and mineral dust deposition has been recorded. A period of high peat accumulation (the HPAE) occurred between c. 5.400–

4550 Cal yr BP, likely driven by a combination of hydrological changes and mineral dust deposition fertilising the bog (Kylander et al., 2018, 2016; Sjöström et al., 2020). The work by Ryberg et al. (2022) modelled the factors that affected species distributions at Store Mosse throughout the last 10.000 years. The results showed a complex interactions between hydroclimate, nutrients and fire (Ryberg et al., 2022). Molecular analysis of bulk peat samples revealed distinct variance in organic compounds and peat decomposition through the Holocene (Martínez Cortizas et al., 2021).

Peat depths reach well over 7 metres. We sampled the oldest, thickest peat section, which lies in the southern arm (Figure 1). In this area, a continuous peat record spanning the Holocene shows a minerogenic fen began forming around 9000 yr BP and evolved into ombrotrophic conditions around 6000 years ago (Kylander et al., 2018; Svensson, 1988). Store Mosse sits on granitic bedrock overlain by glacial lake sediments. A preserved aeolian dune system bisects the bog to the west of the coring site. Surface vegetation today is dominated by *Sphagnum* mosses: *S. fuscum* and *S. imbracatum* on hummucks; *S. magellanicum*, *S. papillosum*, *S. balticum* and *S. cuspidatum* occupy hollows. A variety of graminoids (*Eriophorum* spp., *Rhynchospora alba*), shrubs (*Andromeda* sp., *Vaccinium* spp., *Calluna vulgaris*, *Erica tetralix*) and lichens (*Cladonia* spp.) are common and the bog is ringed by *Betula* and *Pinus silvestris*. Annual average temperature and precipitation are 5.5°C and 800 mm.

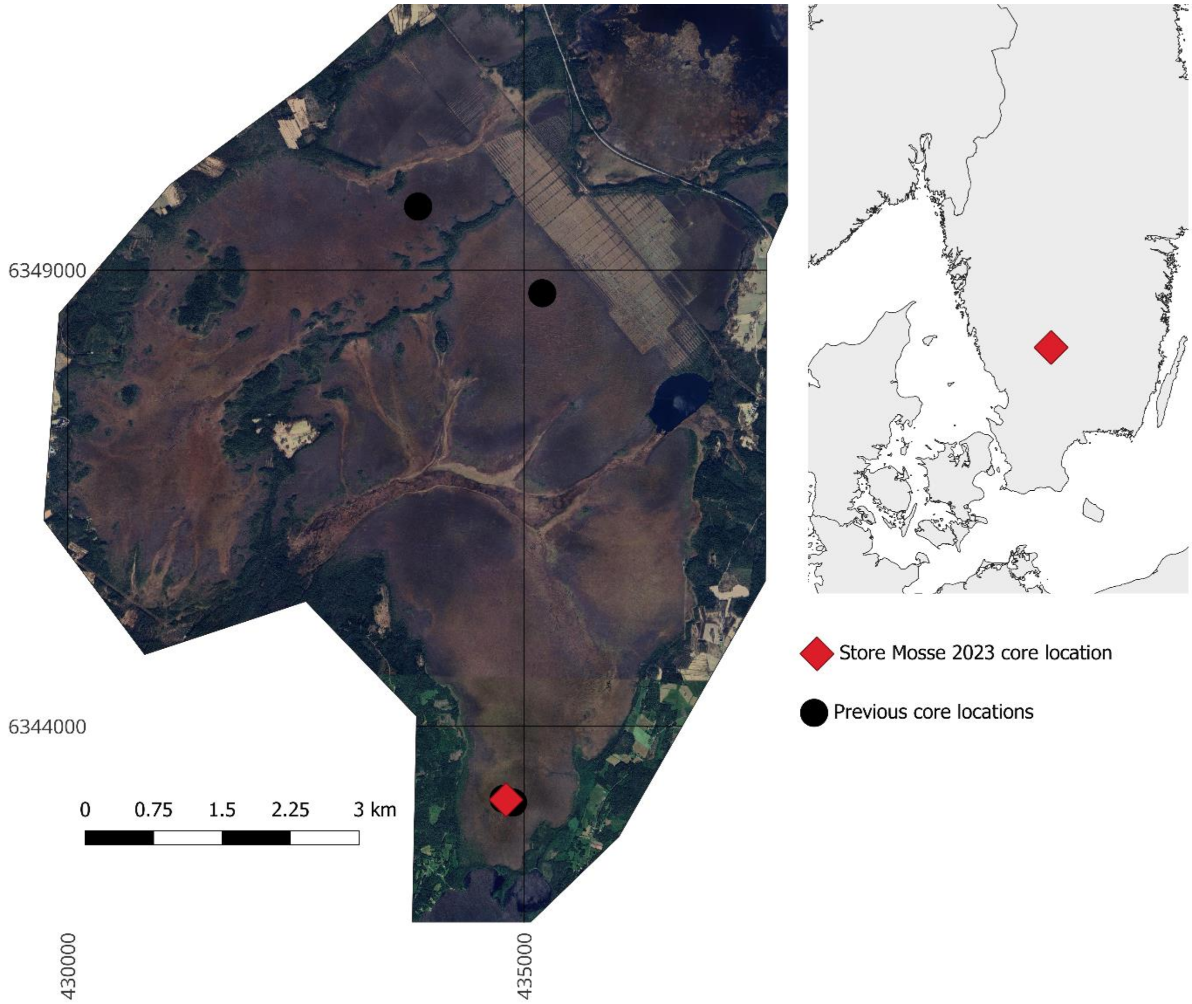

Figure 1. Inset shows the location of Store Mosse in southern Sweden. The core locations for this paper (red) and previous palaeoenvironmental studies (black) overlay satellite imagery of the peatland extent. Earlier coring sites referred to in the text (Kylander et al., 2013; Ryberg et al., 2022) are within 100 metres of our location.

## Methods

### *Peat sampling*

We extracted two parallel peat sequences using a Russian-style corer (1.5 m length; 0.075 m diameter) from a position roughly equidistant between previous coring sites (Kylander et al., 2013; Ryberg et al., 2022; Figure 1). Two drives reached a maximum core depth of 279-cm. The corer was thoroughly washed between drives using a 70% ethanol solution and deionised water. One core was sub-sampled at 2-cm intervals using a serrated knife for physicochemical and palaeoenvironmental analysis. Sample bags were placed on ice in a large cool box and then stored at 4°C upon return to the University of Liverpool.

We targeted the top 200 cm of the second core for microbial analysis selected to span the last 2000 years (Kylander et al. 2013). Samples for DNA sequencing were extracted at 10-cm intervals (first sample at 5-cm depth) using the following protocol to minimise DNA transfer from humans or modern atmospheric input. The exposed peat surface was immediately covered after rotating the core chamber. Wearing sterile gloves, we slid the cover downwards in 10-cm increments, gently scraped off the top 2-mm of peat at each sampling point and cut out a 1 $cm^3$ cube with a scalpel. The blade was sterilised in 70% ethanol, rinsed in deionised water and dried using blue roll between samples. Each peat sample was wrapped in aluminium foil that had been sterilised by placing in an oven at 550°C for 24 hours and then sealed in a screw-top glass vial. All samples were placed in a cool box with crushed ice and stored at -20°C upon return to King's College London. pH was measured immediately after core retrieval, directly on the fresh peat surface of the DNA sampling zones (n=20) with an ExStik pH analyser.

*Physical peat properties*

For the core subsamples bulk density was determined by subsampling the peat gently to fill a 20 ml volumetric syringe taking care to minimise loss of water. Samples were weighed in both wet and dry condition following freeze drying in a Mechatech LyoDry Midi Freeze Dryer Condenser, with the dry masses expressed mg $cm^{-3}$ and water content %. Small subsamples following drying at 105°C overnight were subjected to Loss-on-Ignition (LOI) combustion at 450°C for 4 hours using a Carbolite Gero (30 – 3000°C) furnace.

*Geochronology*

Fresh peat samples were washed and sieved gently (250 µm) using distilled $H_2O$ retaining the coarse fraction. Large plant macrofossils were picked by hand under a low power zoom binocular microscope, the samples were rich with intact *Sphagnum medium* capitulum and *Calluna vulgaris* leaves. The macrofossil samples were prepared to graphite at the NEIF Radiocarbon Laboratory and passed to the SUERC AMS laboratory for $^{14}C$ analysis. The results are reported as conventional radiocarbon years BP (relative to AD 1950) and % modern $^{14}C$, both expressed at the ± 1 σ level for overall analytical confidence. The results have been corrected to $\delta^{13}C$-VPDB‰ = -25 using the $\delta^{13}C$ values provided in the report. The $\delta^{13}C$ value was measured on a dual inlet stable isotope mass spectrometer (Thermo Fisher Delta V) and is representative of $\delta^{13}C$ in the pre-treated sample material. The quoted precision on $\delta^{13}C$ is the uncertainty of repeated measurements of the same $CO_2$ aliquot, i.e. machine error only. Radiocarbon dates and atmospheric metal deposition markers (Table 1) were included in Bayesian age-depth model computed using using ‘rBacon’ (Blaauw et al., 2017; Blaauw and Andrés Christen, 2011).

Table 1. Chronological markers used for Bayesian age-depth modelling of the new Store Mosse peat core. Phases of atmospheric lead (Pb) deposition were taken from Brännvall et al. (2001).

| id. | age | error | depth | %Carbon content | $\delta^{13}$C-VPDB‰ (± 0.1) | Marker |
|---|---|---|---|---|---|---|
| top | -73 | 1 | 0 | | | Surface of peat core |
| Pb peak | -20 | 10 | 13 | | | Peak airfall Pb |
| Base-Pb | 100 | 30 | 31 | | | Modern rise in airfall Pb |
| SUERC-125542 | 303 | 37 | 41 | 43.29 | -26.3 | Sphagnum capitula and branches |
| SUERC-125543 | 673 | 37 | 69 | 43.75 | -24.5 | Sphagnum capitula and branches |
| SUERC-125544 | 882 | 35 | 100 | 44.27 | -25.5 | Sphagnum capitula and branches |
| SUERC-125545 | 1420 | 37 | 150 | 81.53 | -26.9 | Sphagnum stems and Calluna leaves |
| SUERC-125549 | 1858 | 37 | 200 | 37.4 | -25.1 | 3x Sphagnum capitula |
| Roman Pb | 2123 | 50 | 227 | | | Onset of Roman-era Pb mining |

*Geochemistry*

Element concentrations (Na, Mg, Al, Si, P, S, Cl, K, Ca, Ti, V, Cr, Mn, Fe, Co, Ni, Cu, Zn, As, Br, Rb, Sr, Y, Zr, Sn, Sb, I, Ba, Hf, W, Hg and Pb) were determined on a dry mass specific basis, using a Spectro XEPOS 3 Energy Dispersive X-ray fluorescence (XRF) analyser. The samples were hand pressed in 20 mm diameter pots and measured under a He atmosphere under combined Pd and Co excitation radiation and using a high resolution, low spectral interference silicon drift detector. Daily standardisation procedures provide a system check on the XRF analyser, with accuracy verified using 18 certified reference materials (Boyle et al., 2015). Element concentrations (mg g-1) derived by XRF were initially corrected using LOI in the onboard Spectro XEPOS 3 software. Given the very low mineral content the data were reevaluated using normative elements concentrations from the raw element and xray total counts collected by the analyser, and the results ultimately expressed as mass concentrations per unit dry mass (µg $g^{-1}$ or mg $g^{-1}$).

For TOC vapour phase involved de-carbonation using 12N Analar Grade HCl following Yamamuro and Kayanne (1995). The sediment samples were analysed for TOC and TN on a Thermo Scientific Flash Smart Organic Elemental Analyser in the School of Environmental Sciences (University of Liverpool). Two-point daily calibration using Chitin OAS (Elemental Microanalysis Ltd) then analysed twice as an ‘unknown’. Results for the ‘unknown’ were within uncertainty limits of certified value which are Carbon 44.71 % +/- 0.18%, Nitrogen 6.79% +/- 0.15% Certified values were determined by elemental analyser calibrated to Acetanilide 114d from National Institute of Standards and Technology (NIST), Maryland, USA. A series of chitin standards were included at regular intervals throughout the run to monitor drift - again these were all within the uncertainty limits.

### *NIRS Spectroscopy*

Contiguous samples at 20 mm intervals were measured for FT-NIR spectra. The samples were freezed dried, homogenised, hand-pressed and measured on a Bruker MPA spectrometer. All NIRS combined 24 scans collected at 4 $cm^{-1}$ intervals across the range 3595-12500 $cm^{-1}$ focusing on 8000-3800 $cm^{-1}$ as containing the key organic spectral structure. NIRS were converted to 1st derivatives using a centrally weighted 9-point Savitzky-Golay smoothing algorithm minimising noise (Russell et al., 2019). The NIRS for Store Mosse are broadly similar throughout, with the average sample spectra sitting centrally to variations in amplitude. Data-transposed (depths as columns and wavenumbers rows) Principal Components Analysis (tPCA) was conducted across all wavenumbers. tPCA, using the Psych package (R-core, 2020). NIRS were interrogated further using multiple regression of 1st derivative spectra onto end-member spectra derived for known composition materials (Russell et al., 2019). The regression coefficients form the mixing proportions of those components expressed as weight % once adjusted for differing chromatic intensities (Russell et al., 2019). The end member spectra used (Lignin-rich, *Sphagnum,* Humin, Humic; Table S1) and the Store Mosse spectra show few differences, and largely share both peak locations and spectral amplitude.

### *FTIR Spectroscopy*

FTIR Analysis of 69 finely ground peat samples was performed using a Bruker Alpha 2 diamond crystal Attenuated Total Reflectance Fourier Transform Infrared Spectrometer (ATR-FTIR) in the University of Liverpool (UK) Central Teaching Hub. Spectra were retrieved across the mid-infrared region (4000–400 $cm^{-1}$) at a resolution of 4 $cm^{-1}$ by averaging 200 scans per sample. Between samples, the equipment was cleaned with isopropyl alcohol and a background measurement collected. The results were pre-processed in Orange (ver 3.37), which included baseline correction and calculating the average and standard deviation spectrum and 2nd derivative spectra. Following Martínez Cortizas et al. (2024), transposed principal component analysis (tPCA; samples in columns and spectra in rows) was conducted on the processed data.

### *DNA extraction and sequencing*

Total soil DNA was extracted from peat samples using a Macherey-Nagel NucleoSpin Soil DNA extraction kit. All extractions were conducted in the ultra-clean facility at the NERC Environmental Omics laboratory, University of Sheffield. The manufacturer's instructuctions were adapted to a dual-extraction process after extensive testing to identify the optimal sequence of physical and chemical lysis steps to maximise DNA release whilst minimising humic acid contamination. In brief, 500 mg of marginally defrosted peat was scrapped into a 50 mL tube containing lysis beads and pulverised on a Qiagen Tissuelyser after adding the chemical buffer. The supernatant was siphoned in the clean lab and then fresh chemical buffer was added followed by further physical shaking on the Tissuelyser. The second batch of supernatant was extracted and the remaining manufacturer's steps were applied to the combined supernatants.

DNA concentrations and quality were evaluated on a Qubit and a NanoDrop 8000 (Nakayama et al., 2016). DNA was checked spectrophotometrically for purity (260/280 and 260/230 nm ratios). DNA quality was visually inspected by electrophoresis on 0.7% agarose gels. Polymerase chain reaction (PCR) amplification utilised the primers 515F and 806R (Caporaso et al., 2011) targeting the V4 region of bacterial and archaeal 16S rRNA genes. Thermal cycling was slightly tweaked from the manufacturer's protocol after testing. Reactions were conducted in a 20-µL reaction volume with 30 cycles of denaturation at 94°C for 20 s, annealing at 50°C for 60 s and elongation at 72°C for 90 s.

Libraries were sequenced on the Illumina® MiSeq platform (Illumina®, San Diego, USA) using v2 chemistry generating 2 x 250 bp paired-end reads. Reads were processed in QIIME2 2023.9 (Bolyen et al., 2019) and taxonomic assignment was made against Silva v138. Raw sequence pairs were trimmed using 'cutadapt' (Martin, 2011) and then de-noised using the DADA2 tool (Callahan et al., 2016). Taxonomic assignment of the identified amplicon sequence variants was performed using sk-learn (Pedregosa et al., 2011). We processed the genomic data at the Kingdom, Phyla and Class taxonomic levels.

Most plots were generated in RStudio v2024.12.1 using packages ggplot2 v3.5.1 (Wickham, 2016) and tidyPalaeo v0.1.3 (Dunnington et al., 2022). Statistical analysis was performed in R using vegan 2.6.10 (Oksanen et al., 2013).

## Results

### *Peat physical and chemical properties*

Bulk density fluctuates between 0.09 and 0.18 g $cm^{-3}$ (Figure 2). There are several distinct peaks (0 – 25, 45 – 55, 75 – 85, 135 – 140, 155 – 165 cm depth) and a pronounced trough towards the base of the core. Ash content is generally around 1%, with slightly higher percentages between 45 - 55 cm, 135 - 160 cm and a notable increase towards the surface (0 - 25 cm). Peat pH steadily declines from 4.4 in the basal sample to 3.4 near the surface.

Carbon content largely varies between 45% and 51% (mean 48% ± one standard deviation; Figure 2). C% slowly increases with depth. Average nitrogen concentrations are 1.18% (range 0.97 – 1.40%). N and C are moderately correlated (r = 0.36) but higher-amplitude fluctuations in N relative to C mean N:C peaks discriminate intervals where both increase (e.g., 45 – 55 and 80 – 100 cm; Figure S1). Phosphorus concentrations average 162 ppm, with maximum values exceeding 300 ppm measured in the upper 25 cm. P and N are tightly associated (r = 0.84). Their down-core stoichiometric profiles show nutrient enrichment at 0 – 25, 40 - 60, 75 - 100, 125 - 135, 145 – 160 cm (Figure S1). Long-term mean N:C, P:C and P:N ratios are 0.026, 0.0003 and 0.013, respectively.

Minerogenic elements such as Al show maximum values in the upper 25 cm (Figure 2). Subtle deeper peaks (40-60, 75-100, 120-140, 150-165 cm) coincide with elevated P and N concentrations. Indeed, Al and P are tightly associated (r = 0.83). These intervals also correspond to higher density material, so elemental enrichment probably reflects differences in decomposition alongside a mutual source or post-depositional binding. The spike in K in the uppermost 2 cm probably reflects biogenic uptake and recycling by living vegetation.

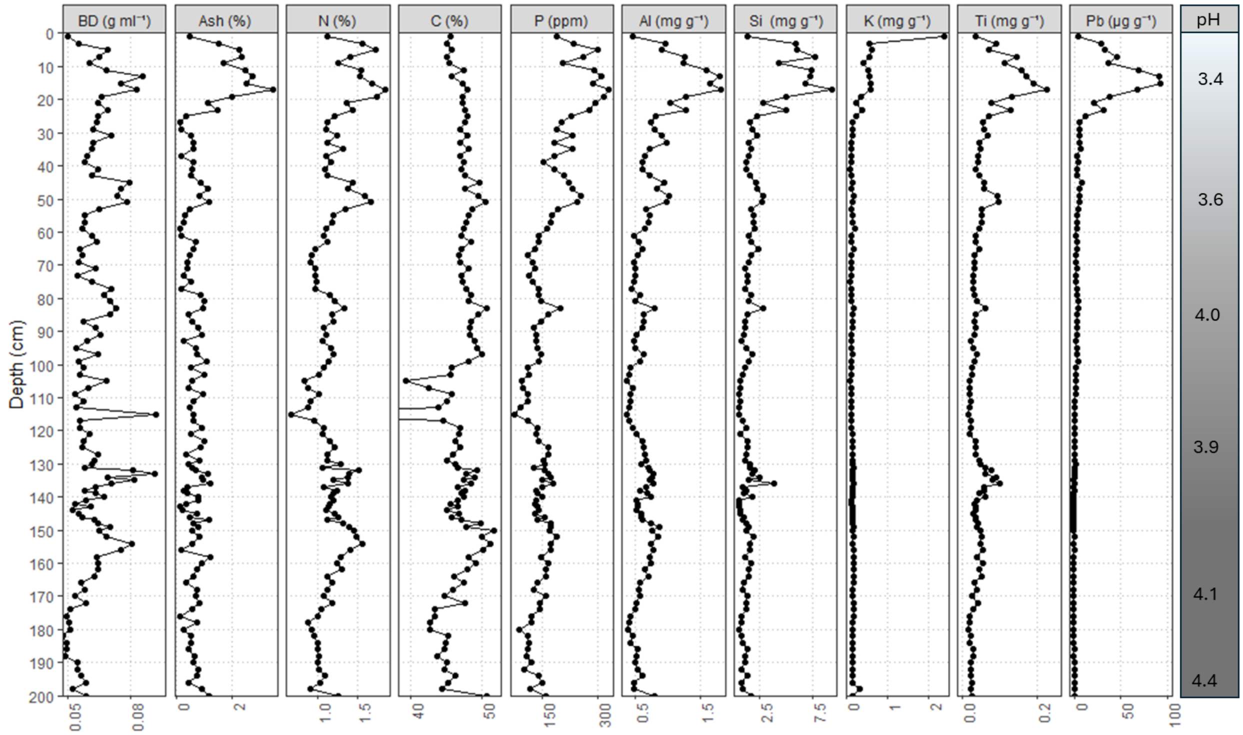

**Figure 2.** Bulk peat properties (pH, bulk density (BD), Ash%) and geochemical profiles.

*NIRS*

NIRS spectra for Store Mosse exhibit peaks and troughs at similar wavelengths and amplitudes (Figure S2). Principal component analysis identified four significant components (CP1-4). CP1 and CP2 explain 52% and 46% of the overall downcore variance, respectively, and their spectral signatures are inversed. The end members used to model the NIRS spectra (Table S1; Russell et al. 2019) show we can confidently ascribe the principal components to discrete vegetation types.

Distinct troughs and peaks characterise the four NIRS end members through the downcore peat profile (Figure 3). CP1 captures the *Sphagnum* component and shows strongly opposing behaviour to CP2, the more heavily decomposed organic material. Notable CP1 troughs / CP2 peaks occur at 10 – 25, 40 – 55, 80 – 100, 130 – 140, 148 – 170-cm depth. The NIRS Lignin end-member is more prevalent between 25 and 100 cm depth compared to the deeper core. This is to some extent opposing behaviour to the NIRS Humic/Fulvic end-member. The NIRS CP3 signal appears to capture dynamics in the active acrotelm (0 – 25 cm), which could be surface nutrient or metal enrichment. Deeper, less distinct, peaks around 50, 130-140 and 150 – 165 cm mimic Al and Ti (Figure 2).

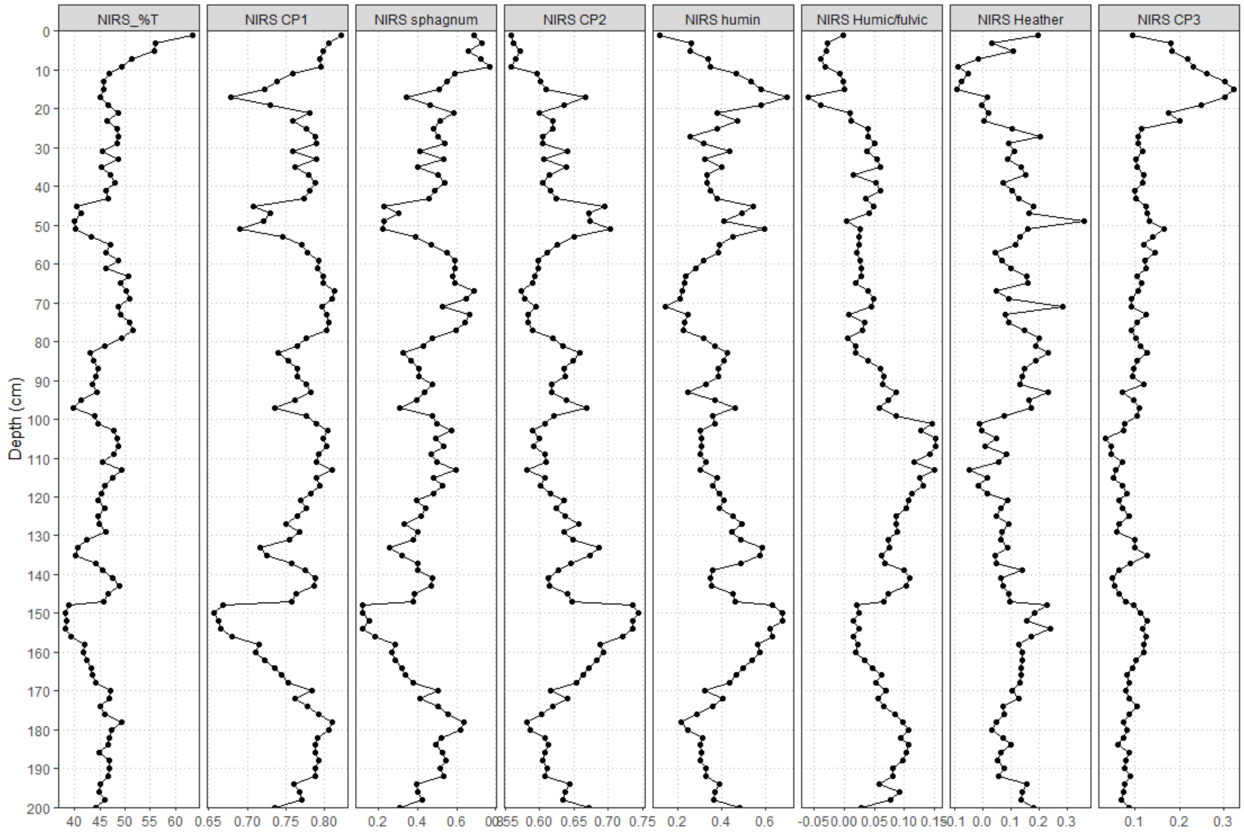

**Figure 3.** NIRS principal components and end-member extraction. NIRS %T represents transmittance: how much light passes through the sample being measured. Lower values likely represent more decomposed and humified (and thus darker) organic matter. NIRS CP1 and NIRS sphagnum represent cellulose-rich plants, especially *Sphagnum* (Table S1). CP2 and NIRS humin show strongly opposing behaviour, evidently capturing more intensely decomposed organic material. NIRS Humic/fulvic represents the Suwanee River Humic and Fulvic Acid international standards and NIRS Heather is a standard from the University of Liverpool NIRS library that captures *Ericaceae* and other lignin-rich material.

### *FTIR*

The average spectra, standard deviation and second derivative are found in the supplementary information (Figure S3). The tPCA analysis will be described here. In total 10 components were extracted in the transposed PCA (tPCA) analysis. The first three components capture 36% (IR_Cp1), 32% (IR_Cp2) and 31% (IR_Cp3) of the variance (Figure 4). The remaining components represent less than 0.7% of the variance. Thus, the focus will be on components 1–5 (Fig. 5). IR_Cp1 displays a broad hump in region I (3600-3000 cm$^{-1}$) associated with OH stretching in hydroxy groups (Table S2). In region II, two distinct peaks occur at 2920 and 2950 $cm^{-1}$ indicative of CH stretching in aliphatic compounds while the peak in region III (1700 $cm^{-1}$) is associated with carboxylic acid (Coward et al., 2019). The peaks in region IV (1630-1615; 1594; 1505 and 1467 $cm^{-1}$) are associated with carboxylic groups together with C=C stretching in aromatic compounds (Chapman et al., 2001; Doskočil et al., 2016; Niemeyer et al., 1992). In region VI a peak occurs between 1300-1200, an area where vibrations from multiple compounds overlap, but the location of the peak centre, at 1251 $cm^{-1}$, indicate that the absorbance may be associated with C-O stretching in acetic esters (Rana et al., 2010). The peaks at 1077, 1030 and 965 $cm^{-1}$ is characteristic for C-O and C-O-C stretching in carbohydrates (Artz et al., 2008; Muthreich et al., 2020).

The second component (IR_Cp2) display elevated scores in region I and VI, with a broad peak noted between 3600-3100 $cm^{-1}$ corresponding to hydroxyl (O-H) vibrations and C-O vibrations in polysaccharides structures (1065, 1045 and 1030 $cm^{-1}$) (Artz et al., 2008; Doskočil et al., 2016). A peak is also noted in region III (1730 $cm^{-1}$), associated with C=O stretching in carbonyl compounds (Zaccone et al., 2007). In region VIII absorbance occur between 635 and 535 $cm^{-1}$, which may be related to multiple compounds, including polysaccharides.

IR_Cp3 display a broad peak in region I (3670-2975 $cm^{-1}$) corresponding to OH stretching and two negative peaks in region II, corresponding to aliphatic structures (2922 and 2855 $cm^{-1}$) in fat, waxes and lipids (Cocozza et al., 2003; Minor and Stephens, 2008; Niemeyer et al., 1992). Starting from region III, IR_Cp3 show the opposite trend to IR_Cp2, with positive peaks in region III (1770-1750 cm-1) corresponding to organic acids in phenolic compounds (Passauer et al., 2012) and IV (1610-1570 cm-1) related to C=C stretching and skeletal vibrations associated with aromatic structures in lignin (Minor and Stephens, 2008; Rana et al., 2010) together with a significant negative peak in region VI (polysaccharides).

IR_Cp4 show a broad peak in region I, between 3300 and 3200 $cm^{-1}$ that may correspond to saturated aliphatic compounds. The distinct peak in region II (2981 $cm^{-1}$) may be associated with methyl ($-CH_3$) or methylene ($-CH_2$) functional groups (Zhang et al., 2016). The presence of these functional groups is further supported by a peak at 1470 $cm^{-1}$, typically also associated with -CH3 or -CH2 vibrations (Rana et al., 2010). In region III, presence of carbonyl compounds is indicated by a peak around 1730 $cm^{-1}$ (Zaccone et al., 2007). In region IV, negative values occur around 1600 $cm^{-1}$, associated with aromatic compounds, together with a peak centred at 1520 $cm^{-1}$, related to NH deformation in secondary amide (Rana et al., 2010). In region V, a peak is observed at 1383 $cm^{-1}$, associated to vibrations in nitrates ($NO_3$) (Minor and Stephens, 2008). In region VI, positive peaks occur at 1290, 1167, 1079 and 904 $cm^{-1}$, while a distinct negative trough occur between 1045 and 990 $cm^{-1}$, associated with C-O stretching in polysaccharides.

IR_Cp5 show a positive peak in region I between 3620-3360 $cm^{-1}$ and a negative trough between 3360-2955 $cm^{-1}$ associated with NH stretching in amines (ref) and C-H stretching in aromatics, respectively (ref). In region II, two distinct peaks are found in the aliphatic compound region (2918 and 2848 $cm^{-1}$) (e.g., Chapman et al., 2001; Artz et al., 2008). In region III, a peak occurs between 1750-1660, with 2nd derivative peaks noted at 1732 and 1714 $cm^{-1}$, indicative of C=O stretching in carbonyl functions (aldehyde, ketones and carboxyl groups) (Cocozza et al., 2003) and C=O stretching in COOH in free organic acids, respectively (Artz et al., 2008). Towards the end of this peak a shoulder is noted between 1685-1660 $cm^{-1}$, associated with C=O stretching in COO groups (Jehlička and Edwards, 2008). In region IV, negative troughs occur around 1600, 1618 and 1506 $cm^{-1}$ respectively, associated with C=C stretching in aromatic compounds in lignin (Doskočil et al., 2016; Zhou et al. 2011). Peaks are also observed at 1470, 1453 and 1385 $cm^{-1}$, which may be associated with multiple compounds, including C-H stretching in aromatics (Minor and Stephens, 2008) and methyl or methylene compounds (Rana et al., 2010). In region V peaks occur at 1385 and 1420 cm-1, associated with phenolic and aliphatic structures (Niemeyer et al., 1992; Senesi et al., 1989), while in region VI a negative trough occur at 1312 $cm^{-1}$, related to syringil breathing in lignin (Rana et al., 2010), followed by positive peaks at 1273 $cm^{-1}$, also associated with lignin (Jääskeläinen et al., 2003) and at 1170, 1080 and 1040 like assoicated with C-O stretching in polysaccharides and carbocylic acids and/or silicate impurities (Viscarra Rossel and Behrens; 2010, Fernandes et al. 2010; Pedersen et al. 2010). A distinct trough is also observed at 971 $cm^{-1}$, which may be associated to silicate minerals. In region VII two additional peaks that may also be associated with minerals are observed at 914 $cm^{-1}$ (Al-OH) 716 $cm^{-1}$ (orthoclase).

Looking down the core (Figure 5), FTIR IR1 and IR2 demonstrate strongly opposing behaviour, with distinct IR1 peaks and IR2 troughs around 15 – 20, 40 – 55, 80 – 100, 133 – 140 and 150 – 160 cm depth. IR3 exhibits more stepped behaviour punctuated by shorter-term variability. Higher phases are observed at 100 – 145 and 155 – 200 cm depth.

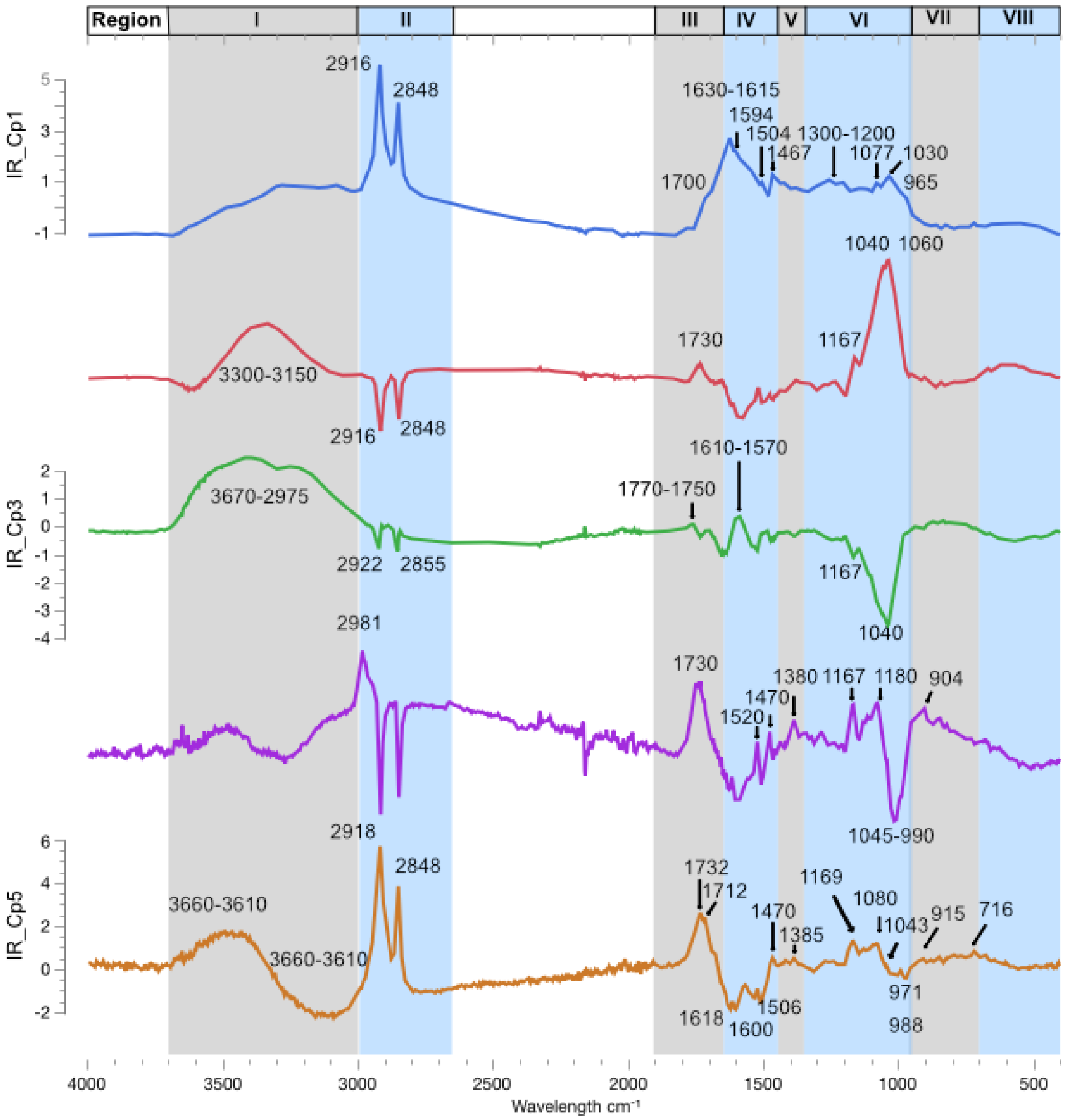

**Figure 4.** Components 1–5 of the tPCA analysis. The spectra are divided into eight (I-VIII) regions and significant peaks for each component are labelled.

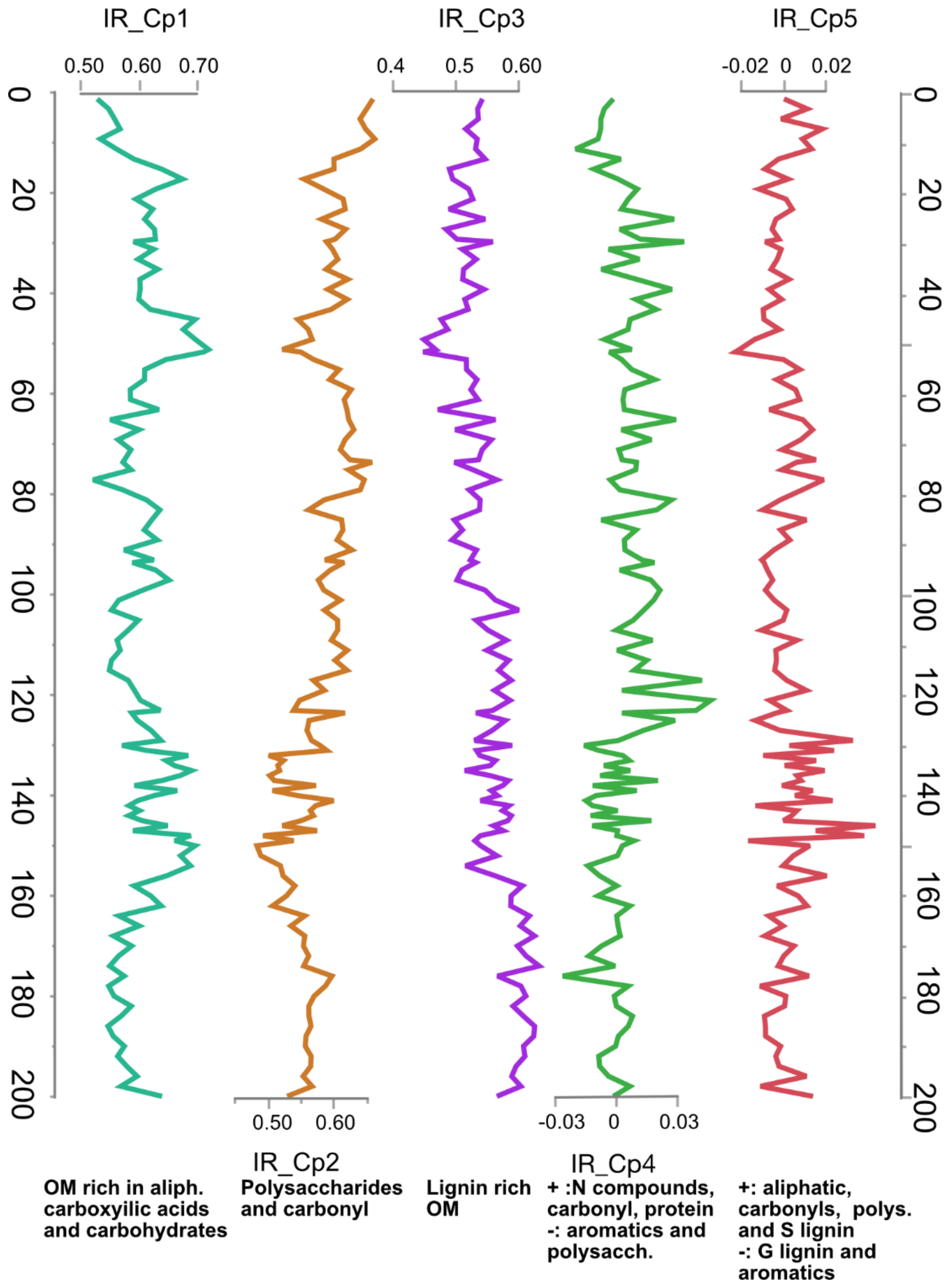

**Figure 5.** Down-core stratigraphies of the five rotated FTIR component scores, including information on what organic compounds each component represent.

*Microbial stratigraphy*

Bacteria comprise the bulk (mean 84%) of the prokaryote community at Store Mosse (Figure S4). Bacteria dominate the upper 50 centimetres and between 95 and 165-cm depth. Somewhat higher proportions of archaea (>20%) occur at 55-85 cm and below 165-cm. The most abundant bacteria phyla, in order, are Acidobacteria (31.4%), Verrucomicrobiota (16.5%), Actinobacteriota (10.8%), Proteobacteria (10.0%), Desulfobacterota (7.7%), Chloroflexi (7.4%) and Planctomycetota (6.9%) (Figure 6). Other phyla present in abundances greater than 1% are Firmicutes, Methylomirabilota, Spirochaetota, Bacteroidota and FCPU426. Most archaea are from the phlyum Crenarchaeota (78.1%). Halobacterota (13.5%) and Thermoplasmatota (8.1%) are the only other archaea with notable abundances.

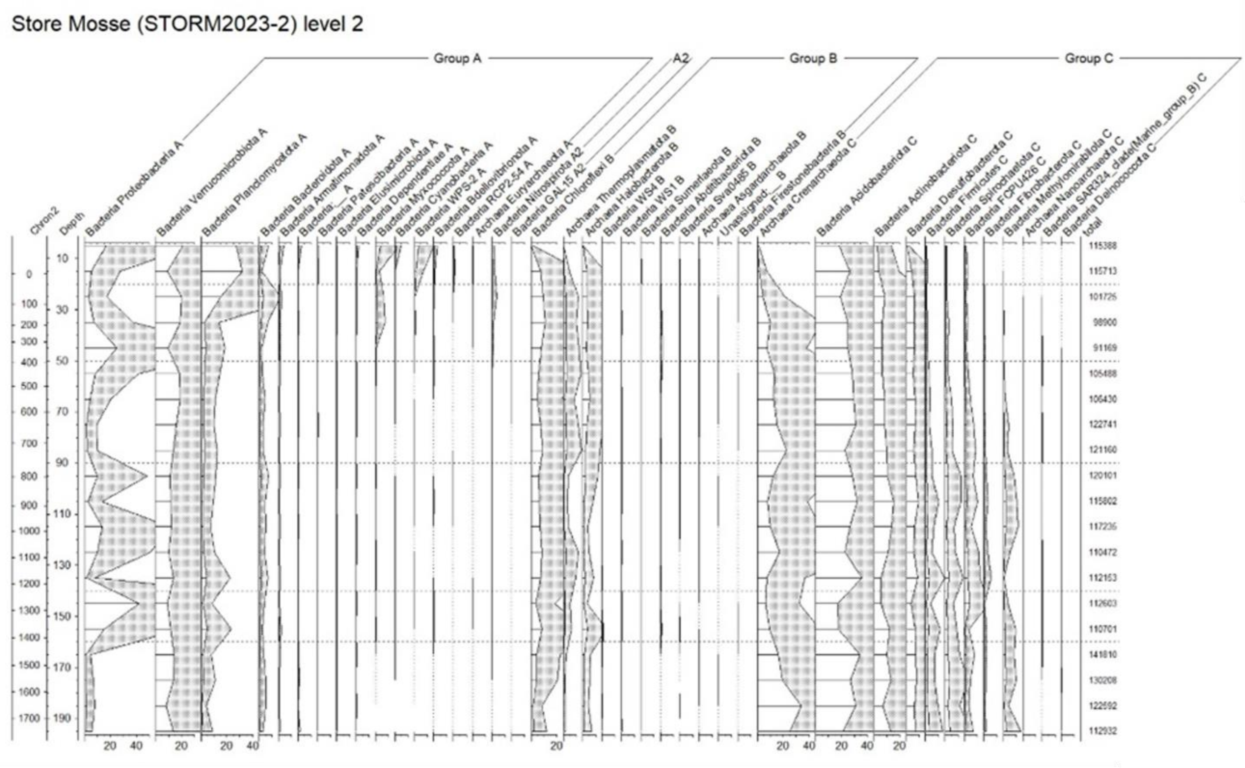

**Figure 6.** Tilia plot of the Store Mosse bacteria and archaea phyla through the Store Mosse core.

Alpha diversity metrics, especially phyla OTUs, indicate slow decline in diversity with depth (Figure S5). The likely transition zone from from aerobic to anaerobic conditions (25-35 cm) shows particularly high diversity. Peaks in Shannon diversity are also present at 95, 125 and 155-cm. The down-core decline in diversity is more visible at higher taxonomic levels.

A number of taxa exhibit striking stratigraphic variation (Figure 6, Figure S6). First, some bacteria appear almost exclusively near the surface (5 - 15 cm), including *WPS-2*, *Cyanobacteria*, *Bdellovibrionata* and *RCP2-54*. *Planctomycetota* is present throughout the core and most abundant (up to 40%) in the upper 35 cm. Phyla that are most abundant in the upper 50-cm include *Bacteroidata*, *Myxcocotta* and *Nitrospirota*. These are captured by Group A in Figure 6. Group B contains phyla such as *Chloroflexi* and *Halobacterota* that are present in modest abundances throughout the core except near the bog surface. Group C comprises phyla that are present at most depths but generally in the highest proportions below 100-cm (e.g., *Acidobacteria*, *Actinobacteria*, *Desulfobacterota*, *Firmicutes*, *Spirochaeotato*, *Methylomirabilota*. For archaea, *Euryarchaeota* is present in the surface layers (0-30 cm) at all sites. *Thermoplasmotata* and especially *Halobacterota* dominate 20-40 cm and then are steadily replaced by *Crenarchaeota* with depth. *Thermoplasmotata* and *Halobacterota* have a phase of greater abundance (25%) at 130 - 160 cm.

Given nutrient concentration and decomposition intensity fluctuates quite markedly down the core, we are particularly interested in phyla that illustrate comparable shorter-term fluctuations. *Proteobacteria* does so most vividly, with distinct peaks in abundance at 5-15, 35 – 55, 85 – 105, 115-125 and 145-155 cm (Figure 6). By contrast, several major taxa including Acidobacteria, Verrumicrobiota and Firmicutes decrease in abundance at the same depths (Figure S6). The peaks in proteobacteria predominantly constitute class *Gammaproteobacteria (*Order *Burkholderiales)*, other than the shallowest peak which is mostly *Alphaproteobacteria*. Moreover, each depth with high *Proteobacteria* abundance plots in different ordination space to horizons with low abundance (Figure S7). So, the stratigraphic variance captures microbial community dynamics rather than being restricted to select taxa.

### *Multi-proxy profiles*

Strong congruence was observed between multiple proxies of peat decomposition. NIRS transmission (%T), NIRS Principal Component 1 and FTIR Principal Component 2 show strong, positive correlations (Figure 3; Figure 7; Figure S8). FTIR CP2 captures changes in polysaccharides, and thus the strong similarity with the *Sphagnum* NIRS end member is logical. Showing opposing behaviour are the second NIRS component and FTIR component 1, which reflects aliphatic compounds. These co-vary tightly with the humic (well-decomposed) NIRS end member. These two groupings of organic compounds are picked out distinctly by the second PCA component (Table 2). Together, the down-core behaviour illustrates distinct shifts between *Sphagnum*-rich and *Sphagnum*-poor phases over the last 2000 years. This shift in the dominant vegetation has strong effects on decomposition efficiency. Less acidic pH towards the surface is a common pattern in ombrotrophic bogs but this effect will not explain the fine-resolution stratigraphy.

Importantly, most marked shifts from *Sphagnum*-dominated to well-humified peat occur in tandem with *Proteobacteria* peaks and higher microbial community diversity (Figure 7; Figure S7). These associations are most evident at 40 – 60 cm, 85 – 100 and 140 – 160 cm depth. The *Proteobacteria* spike at 110 – 130 cm aligns less strongly with a decomposition response, however.

**Table 2.** Loadings for scaled variables from Principal Component Analysis of the Store Mosse core. Variables in bold black font denote positive correlations (>0.2) and dark grey font show negative associations (< -0.2).

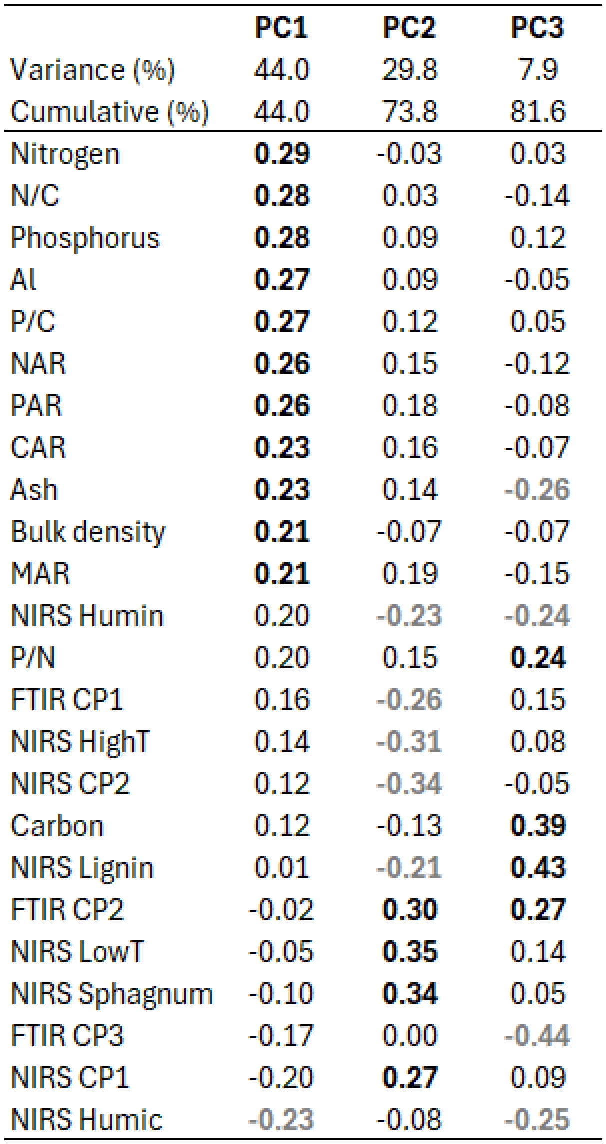

| | **PC1** | **PC2** | **PC3** |
|---|---|---|---|
| Variance (%) | 44.0 | 29.8 | 7.9 |
| Cumulative (%) | 44.0 | 73.8 | 81.6 |
| Nitrogen | **0.29** | -0.03 | 0.03 |
| N/C | **0.28** | 0.03 | -0.14 |
| Phosphorus | **0.28** | 0.09 | 0.12 |
| Al | **0.27** | 0.09 | -0.05 |
| P/C | **0.27** | 0.12 | 0.05 |
| NAR | **0.26** | 0.15 | -0.12 |
| PAR | **0.26** | 0.18 | -0.08 |
| CAR | **0.23** | 0.16 | -0.07 |
| Ash | **0.23** | 0.14 | -0.26 |
| Bulk density | **0.21** | -0.07 | -0.07 |
| MAR | **0.21** | 0.19 | -0.15 |
| NIRS Humin | 0.20 | -0.23 | -0.24 |
| P/N | 0.20 | 0.15 | **0.24** |
| FTIR CP1 | 0.16 | -0.26 | 0.15 |
| NIRS HighT | 0.14 | -0.31 | 0.08 |
| NIRS CP2 | 0.12 | -0.34 | -0.05 |
| Carbon | 0.12 | -0.13 | **0.39** |
| NIRS Lignin | 0.01 | -0.21 | **0.43** |
| FTIR CP2 | -0.02 | **0.30** | **0.27** |
| NIRS LowT | -0.05 | **0.35** | 0.14 |
| NIRS Sphagnum | -0.10 | **0.34** | 0.05 |
| FTIR CP3 | -0.17 | 0.00 | -0.44 |
| NIRS CP1 | -0.20 | **0.27** | 0.09 |
| NIRS Humic | -0.23 | -0.08 | -0.25 |

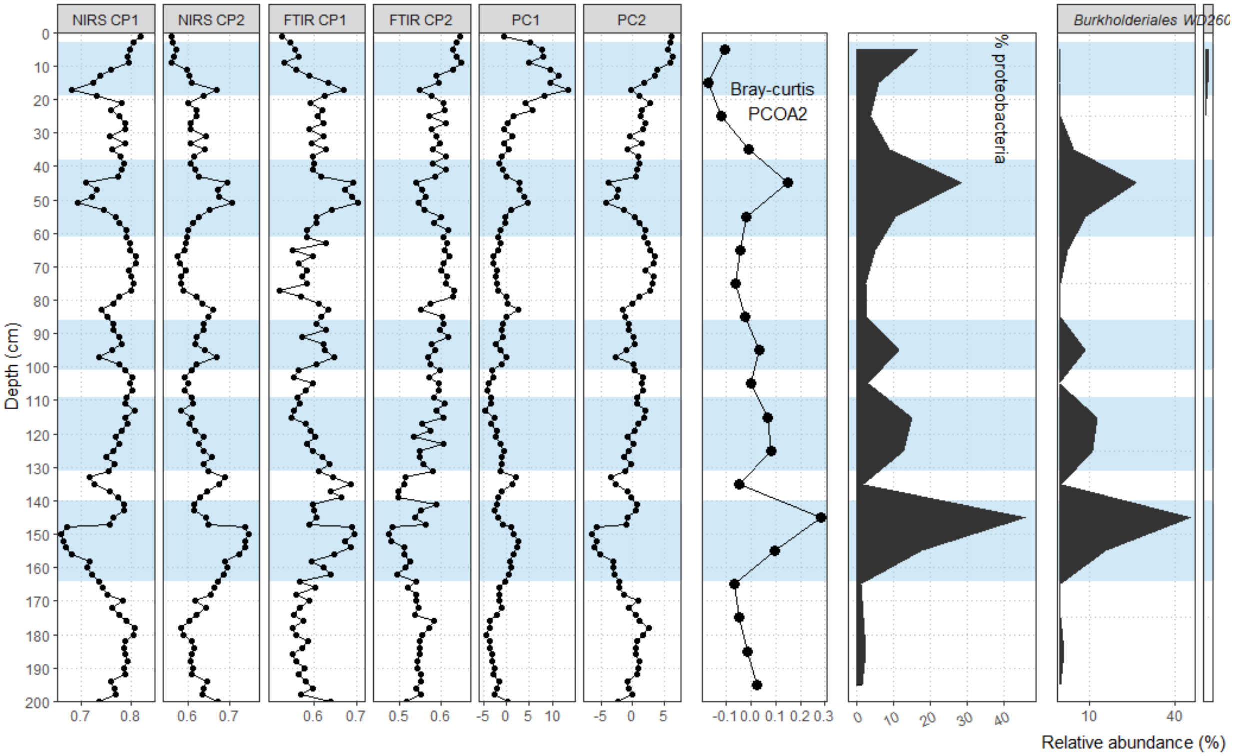

**Figure 7.** Down-core profiles demonstrating strong alignment between NIRS and FTIR measures of decomposition and microbial taxa. PC1 and PC2 are the two primary components from PCA analysis of the full multi-proxy dataset. Bukholderialies and WD260 are the dominant Classes of Order Gammaproteobacteria, which in turn represents the major taxa of phyla *Proteobacteria*. Higher Bray-Curtis dissimilarity values imply greater microbial diversity.

*Age-depth modelling*

The $^{14}$C ages along with markers for near surface regional airborne pollution and an age of 2023 for the peat surface form a conformable sequence (Table 1; Figure 8A). The age markers were incorporated in a Bayesian age-depth model (Table 1) using ‘rBacon’ (Christen et al., 2009; Blaauw et al., 2011) operating in the R environment (R Core Team, 2017). The Markov chain Monte Carlo repetitions were constrained by a gamma distribution with mean 10 a. cm$^{-1}$ and shape 1.7 and a beta distribution with mean 0.5 and shape 8. The Bacon age-depth model shows the microbial analysis (deepest sample at 195 cm) spans the last 1800 years (Figure 8A). The three Pb markers nicely reinforce the radiocarbon profile. Extrapolating below the radiocarbon ages, supported by the Roman Pb marker, places the basal core depth (279 cm) at 2650 cal yr BP.

Long-term peat accumulation appears to have been relatively constant (19.8 ± 4.1 yr / cm (mean ± standard deviation)) before the expected rapid accumulation towards the bog acrotelm. Peat mass accumulation rates (Peat MAR) generally range between 50 and 100 g $m^{-2}$ $y^{-1}$ (Figure 8B). Carbon accumulation rate (CAR) at Store Mosse over the last 2000 years is high: 34.2 ± 11.9 g $m^{-2}$ $y^{-1}$. The mean below 25 cm (so excluding the high apparent rates) is 31.0 ± 7.1 g $m^{-2}$ $y^{-1}$. As well as rapid apparent rates in the acrotelm, earlier periods of fast carbon accumulation occurred around 300 – 420, 600 – 820, 1150 – 1200, 1300 – 1450 and 1700 – 1800 cal yr BP. Nitrogen and phosphorus accumulation rates exhibit similar profiles. Mean NAR and PAR below 25 cm are 0.74 ± 0.23 g $m^{-2}$ $y^{-1}$ and 9.51 ± 3.22 mg $m^{-2}$ $y^{-1}$, respectively.

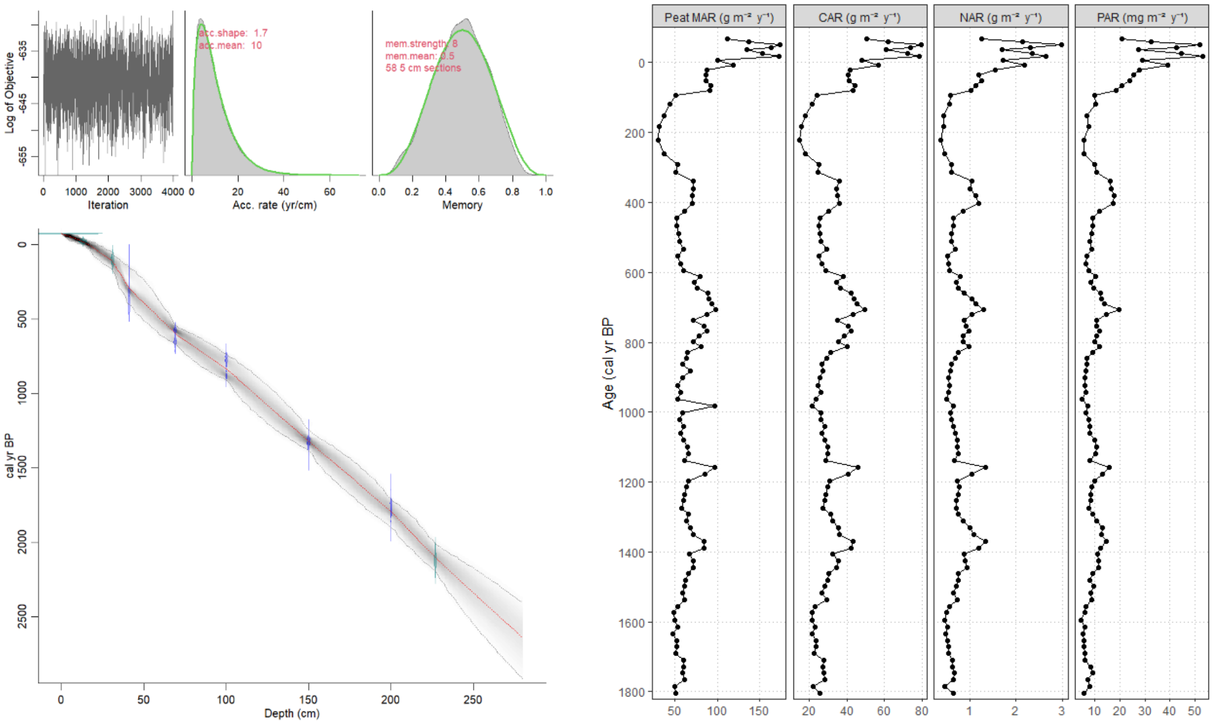

**Figure 8.** (A) Age-depth model and (B) peat and nutrient accumulation rates. The model was run for the full core (275-cm depth) but profiles are cut off at 200-cm to enable comparison with the microbial DNA data, where the deepest sample was 195 cm.

## Discussion

### *Late-Holocene Store Mosse microbial communities*

The dominant bacterial phyla at Store Mosse are *Proteobacteria* and *Acidobacteria* (Figure 6). This is common across northern peatlands (Aksenov et al., 2021; Concheri et al., 2017; Li et al., 2022; Lin et al., 2014a; Richy et al., 2024; Seward et al., 2020; Tsitko et al., 2014; Tveit et al., 2013; Wood et al., 2021). These taxa can tolerate low pH, nutrient-poor conditions (Pankratov et al., 2011). Relative abundance of these phyla does appear to differ regionally, and potentially on a site-specific basis but there are currently too few studies to judge. For example, *Acidobacteria* averages 26% (max 36%) of total abundance at Store Mosse, comparable to a bog in the Pyrenees (Richy et al., 2024) but much higher than 9% in a deep-peat sample from Italy and below the 50% of community composition sequenced in Minnesota, USA (Lin et al., 2014). A study of 39 fens Europe showed *Proteobacteria* abundance varied between 15 and 50% based on depth and wetness (Emsens et al., 2020). Other phyla present in moderate abundances at Store Mosse are common to most studied ombrotrophic peatlands but there is notable stratigraphic variance. For example, Birnbaum et al. (2023) and Bai et al. (2018) observed high *Chloroflexi* in the acrotelm, whereas this is taxa is present at most depths in Store Mosse other than the near-surface. The main archaeal phylum at Store Mosse is *Crenarchaeota*, with some presence of *Euryarchaeota*. Both are common in northern peatlands. There is, however, no sequenced *Thaumarchaeota* at Store Mosse, as reported for temperate peatlands in China (Li et al., 2022). Alpha diversity metrics and phyla OTUs decrease along the vertical gradient (Figure S5), although not on the scale observed in other northern peatlands (Dedysh et al., 2006; Jaatinen et al., 2007; Morales et al., 2006). We found maximum prokaryote richness and Shannon diversity at 25-35 cm depth, which would correspond with the 'biodiversity hotspot' reported elsewhere for ombrotrophic peatlands (Andersen et al., 2013; Birnbaum et al., 2023; Clymo and Bryant, 2008; Puglisi et al., 2014). The preponderance of *Alphabacteria* (Class *Rhizobiales* towards the surface of Store Mosse (Figure S6) presumably relates to its importance in *Sphagnum* biochemical functioning (Kolton et al., 2022). Our finding that *Proteobacteria* peaks are dominated by Order *Gammaproteobacteria* (Class *Burkholderiales)* is intriguing. *Gammaproteobacteria* are r-strategists, so depend on relative nutrient enrichment (Mastný et al., 2021) compared to other taxa.

### Microbe-vegetation-nutrient interactions are associated with long-term carbon accumulation

The alternating behaviour between two main vegetation components aligns with experimental studies showing notable differences in decomposition rate between *Sphagnum* and vascular plants such as *Carex* and *Eriophorum* (Aerts et al., 2001, 1999;

Pankratov et al., 2011). This likely reflects the greater presence in *Sphagnum*-dominated litter of phenolic substances. These substances show marked resistant to decomposition by inhibiting microbial enzymes (Fenner and Freeman, 2011; Verhoeven and Liefveld, 1997). Plant macrofossil data from Ryberg et al. (2022) showed that a key feature of Store Mosse's development over the last 2000 years is the periodic replacement of *Sphagnum* by vascular plants (Figure S9). We observe in our study that community microbial diversity at Store Mosse follows this pattern (Figure 7) and that total bacterial abundance is generally higher in sedge-dominated peat (Figure S10).

Our primary research question is whether the interplay between microbial activity and vegetation can be linked first to nutrient cycling and then, ultimately, to carbon accumulation through time. Phosphorus and nitrogen accumulation rates are higher during most phases of low PC2 (i.e., less *Sphagnum*) loadings (Figure 9). N deposition effects on microbial communities are well studied (e.g., Blaud et al., 2015; Bragazza et al., 2012). Less is known about the role of P, although a recent field experiment showed *Sphagnum* inhibition under high-P addition (Lu et al., 2022). Most field studies report a reduction in *Sphagnum* under higher nutrient input (Bubier et al., 2007; Fritz et al., 2012; Gunnarsson et al., 2004) because an excess of nutrients becomes available in the acrotelm, enabling vascular plants to take hold. In turn, the dominant microbial taxa will tend to shift target to the labile litter of vascular plants. At Store Mosse, *Proteobacteria* peaks largely constitute *Gammaproteobacteria*. which have been identified as a lignin-degrading taxa (Bugg et al., 2011; Dom et al., 2021) and, as r-strategists, require ample nutrient enrichment (Mastný et al., 2021). Furthermore, higher *Gammaproteobacteria* abundance under *Ericaceae* treatment was observed in a mesocosm experiment (Romanowicz, 2013). At the same time, *Sphagnum* has a distinctive cellular composition and breakdown process. Its high polyphenolic content means cell walls decompose slowly, providing more time for nutrient mineralisation (Hájek et al., 2011). This fits our findings: high-*Proteobacteria*, shrub and phosphorus accumulation rates are associated whilst the *Sphagnum*-dominated intervals exhibit lower P content. This reflects the lower bulk density (Figure 3) of *Sphagnum* due to its polysaccharide (FTIR CP2; Figure 7) and phenolic content and thus less efficient decomposition. Strong associations between P and N concentrations and Bray-Curtis dissimilarity ($r^2 > 0.5$; Figure S11) are further evidence of interplay between nutrients and microbial diversity. Interestingly, PC3 also seems to capture the rising P:N stoichiometry since 900 cal yr BP (100-cm depth), alongside higher NIRS lignin and lower NIRS humic/fulvic loadings (Figure 3; Figure 9). This behaviour is then overprinted by the flips between *Sphagnum* and vascular taxa.

Carbon accumulation generally shows similar down-core associations. Most intervals of elevated carbon accumulation over the last 2000 years coincide with the highlight phases of high *Proteobacteria* abundance and microbial diversity, high P accumulation and elevated P:C and replacement of *Sphagnum* by sedges (Figure 9; Figure S9). This is consistent with previous studies, whereby higher microbial diversity promotes decomposition (Richy et al., 2024; Seward et al., 2020; St. James et al., 2021). At Store Mosse this behaviour maps particularly nicely across proxy and microbial stratigraphies at 220 – 420 and 670 – 850 cal yr BP. A similar story occurs between 1200 and 1400 yr BP, albeit with an offset that could be explained by differences in sampling resolution between metabarcoding and other proxies. Similarly, we may have missed the short-lived peak in CAR at 1150 – 1200 cal yr BP due to the 10-cm sampling resolution of our bacterial data. Alternatively (or in addition), evidence of fires around 1200 cal yr BP (Figure S10; Ryberg et al. 2022) could explain the very high bulk density of this material. The interval between 950 and 1100 yr BP is different. There is a peak in *Proteobacteria* abundance, but responses amongst proxies are muted. One explanation is the major transition in *Sphagnum* species at this time (Kylander et al., 2018; Ryberg et al., 2022). An alternative proposition is non-linear biogeochemical behaviour. This high-*Proteobacteria*, low-CAR zone occurs at the end of sustained (~450 years) elevated P accumulation. This may have slowly shifted the bog's nutrient limitation status, perturbing the long-term balance between primary productivity and microbial decomposition. Non-linear responses have been observed for peatlands, usually in the form of rapid carbon accumulation after abrupt, high-magnitude nutrient input from dust (Kylander et al., 2018; Sjöström et al., 2022, 2020) or tephra (Ratcliffe et al., 2020). Our recent conceptual model (Schillereff et al., 2021) postulated that long-term nutrient input would ultimately reduce carbon accumulation. Our Store Mosse data could be mechanistic evidence of this outcome.

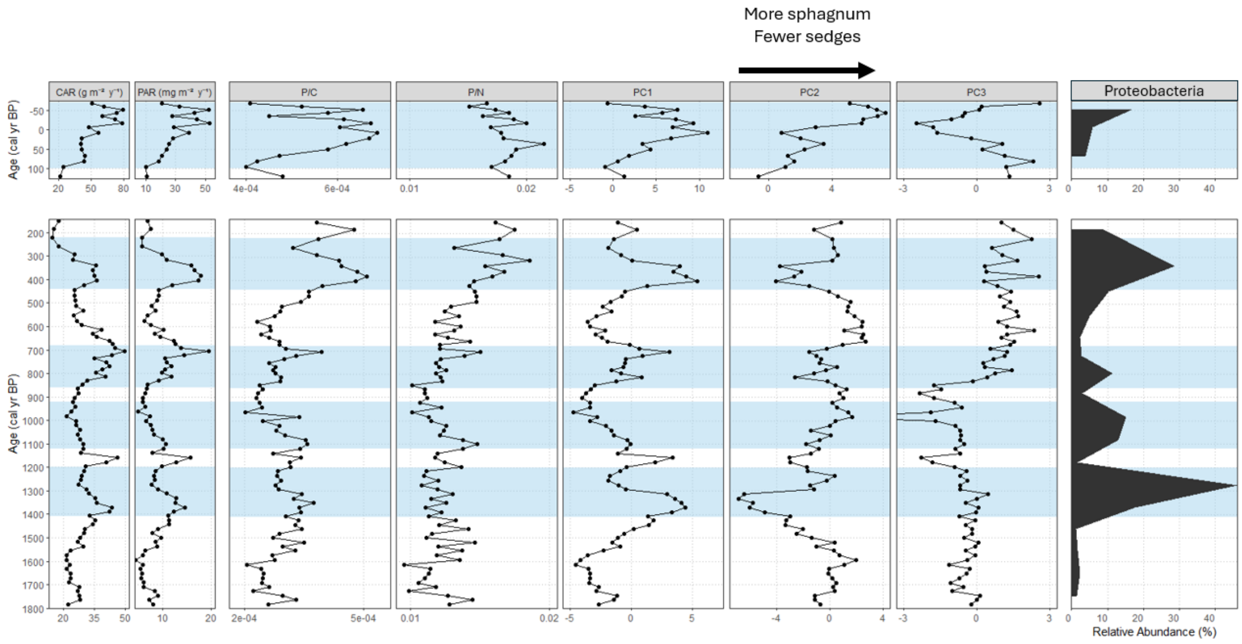

**Figure 9.** Carbon (CAR) and phosphorus (PAR) accumulation rates plotted against stoichiometric ratios, PCA components and Proteobacteria abundance over the last 1800 years at Store Mosse. Blue zones are horizons with high *Proteobacteria* abundance. Note some x-axis ranges different between the top row and bottom row for visualisation purposes.

Comparing our data to the extensive palaeoenvironmental literature from Store Mosse, we calculated somewhat higher rates of carbon accumulation (31.0 ± 7.1 g $m^{-2}$ $y^{-1}$) to Kylander et al. (2018; 22.8 ± 10.6 g $m^{-2}$ $y^{-1}$) for the overlapping period of our studies. Our average carbon contents are very similar: 46.9 ± 2.1% to 46.6 ± 1.3%. So, the CAR difference almost certainly arises from our respective approaches to calculating bulk density. We filled a syringe of known volume rather than estimating the volume of each core slice. Our CAR values at the high end of the time-weighted average for northern peatlands (Loisel et al., 2014), which implies the importance of using a consistent method to determine bulk density may be underappreciated.

## Conclusion

Our study of interacting nodes at Store Mosse finds evidence of strong associations between carbon accumulation, phosphorus content, microbial diversity and vegetation over the last 2000 years. This relationship breaks down on occasion, potentially driven by non-linear responses to long-term nutrient input. Future investigations should delve deeper by reconstructing multiple carbon cycle nodes at many more temperate peatlands. A more complete mechanistic understanding probably also necessitates the development of a process-based model that explicitly simulates carbon and nutrient dynamics. Moreover, our findings underscore the importance of peatland research leveraging the increasing recognition of environmental DNA within global research agendas.

## Acknowledgements

We are grateful to many colleagues who have supported our research. We received exceptional technical support whilst working at the NERC Environmental Omics Facility from Tom Holden, Lucy Knowles and Gavin Horsburgh. Thank you to Sabena Blackbird, Joshua Hicks and Luke Glascott for conducting some of the laboratory analyses. We thank Petter Hällberg (Stockholm University) for participating in fieldwork and Eleanor Ryberg (Queens University, Belfast) for sharing plant macrofossil data and Antonio Martínez Cortizas (Universidade de Santiago de Compostela) for advice on processing and interpreting FTIR data. We thank Carina Härlin for help with logistics and permissions to core and the County of Jönköping is thanked for granting access to sample in Store Mosse National Park. This project was funded by the Natural Environment Research Council (NE/X010635/1). J. Sjöström was also funded by PollutedPast (ERC-101087832).

## References

A global multiproxy database for temperature reconstructions of the Common Era, 2017. . Sci Data 4, 170088. https://doi.org/10.1038/sdata.2017.88

Aerts, R., Verhoeven, J.T.A., Whigham, D.F., 1999. Plant-Mediated Controls on Nutrient Cycling in Temperate Fens and Bogs. Ecology 80, 2170–2181. https://doi.org/10.1890/0012-9658(1999)080[2170:PMCONC]2.0.CO;2

Aerts, R., Wallen, B., Malmer, N., 1992. Growth-Limiting Nutrients in Sphagnum-Dominated Bogs Subject to Low and High Atmospheric Nitrogen Supply. The Journal of Ecology 80, 131. https://doi.org/10.2307/2261070

Aerts, R., Wallén, B., Malmer, N., De Caluwe, H., 2001. Nutritional constraints on Sphagnum-growth and potential decay in northern peatlands. Journal of Ecology 89, 292–299. https://doi.org/10.1046/j.1365-2745.2001.00539.x

Aksenov, A.S., Shirokova, L.S., Kisil, O.Y., Kolesova, S.N., Lim, A.G., Kuzmina, D., Pouillé, S., Alexis, M.A., Castrec-Rouelle, M., Loiko, S.V., Pokrovsky, O.S., 2021. Bacterial Number and Genetic Diversity in a Permafrost Peatland (Western Siberia): Testing a Link with Organic Matter Quality and Elementary Composition of a Peat Soil Profile. Diversity 13, 328. https://doi.org/10.3390/d13070328

Andersen, R., Chapman, S.J., Artz, R.R.E., 2013. Microbial communities in natural and disturbed peatlands: A review. Soil Biology and Biochemistry 57, 979–994. https://doi.org/10.1016/j.soilbio.2012.10.003

Anderson, D.E., 2002. Carbon accumulation and C/N ratios of peat bogs in North-West Scotland. Scottish Geographical Journal 118, 323–341. https://doi.org/10.1080/00369220218737155

Artz, R.R.E., Chapman, S.J., Robertson, A.H.J., Potts, J.M., Laggoun-Défarge, F., Gogo, S., Comont, L., Disnar, J.-R., Francez, A.-J., 2008. FTIR spectroscopy can predict organic matter quality in regenerating cutover peatlands. Soil Biology and Biochemistry 40, 515–527.

Bai, Y., Wang, J., Zhan, Z., Guan, L., Jin, L., Zheng, G., Huang, Z., 2018. The Variation of Microbial Communities in a Depth Profile of Peat in the Gahai Lake Wetland Natural Conservation Area. Geomicrobiology Journal 35, 484–490. https://doi.org/10.1080/01490451.2017.1392651

Basiliko, N., Moore, T.R., Jeannotte, R., Bubier, J.L., 2006. Nutrient Input and Carbon and Microbial Dynamics in an Ombrotrophic Bog. Geomicrobiology Journal 23, 531–543. https://doi.org/10.1080/01490450600897278

Beilman, D.W., MacDonald, G.M., Smith, L.C., Reimer, P.J., 2009. Carbon accumulation in peatlands of West Siberia over the last 2000 years. Global Biogeochemical Cycles 23. https://doi.org/10.1029/2007GB003112

Belyea, L.R., Malmer, N., 2004. Carbon sequestration in peatland: patterns and mechanisms of response to climate change: CARBON SEQUESTRATION IN PEATLAND. Global Change Biology 10, 1043–1052. https://doi.org/10.1111/j.1529-8817.2003.00783.x

Birnbaum, C., Wood, J., Lilleskov, E., Lamit, L.J., Shannon, J., Brewer, M., Grover, S., 2023. Degradation Reduces Microbial Richness and Alters Microbial Functions in an Australian Peatland. Microb Ecol 85, 875–891. https://doi.org/10.1007/s00248-022-02071-z

Blaauw, M., Andrés Christen, J., 2011. Flexible Paleoclimate Age-Depth Models Using an Autoregressive Gamma Process. Bayesian Analysis 6, 457–474. https://doi.org/10.1214/11-BA618

Blaauw, M., Christen, J.A., Aquino Lopez, M.A., 2017. rbacon: Age-Depth Modelling using Bayesian Statistics. CRAN: Contributed Packages. https://doi.org/10.32614/cran.package.rbacon

Blaud, A., Phoenix, G.K., Osborn, A.M., 2015. Variation in bacterial, archaeal and fungal community structure and abundance in High Arctic tundra soil. Polar Biol 38, 1009–1024. https://doi.org/10.1007/s00300-015-1661-8

Bolyen, E., Rideout, J.R., Dillon, M.R., Bokulich, N.A., Abnet, C.C., Al-Ghalith, G.A., Alexander, H., Alm, E.J., Arumugam, M., Asnicar, F., Bai, Y., Bisanz, J.E., Bittinger, K., Brejnrod, A., Brislawn, C.J., Brown, C.T., Callahan, B.J., Caraballo-Rodríguez, A.M., Chase, J., Cope, E.K., Da Silva, R., Diener, C., Dorrestein, P.C., Douglas, G.M., Durall, D.M., Duvallet, C., Edwardson, C.F., Ernst, M., Estaki, M., Fouquier, J., Gauglitz, J.M., Gibbons, S.M., Gibson, D.L., Gonzalez, A., Gorlick, K., Guo, J., Hillmann, B., Holmes, S., Holste, H., Huttenhower, C., Huttley, G.A., Janssen, S., Jarmusch, A.K., Jiang, L., Kaehler, B.D., Kang, K.B., Keefe, C.R., Keim, P., Kelley, S.T., Knights, D., Koester, I., Kosciolek, T., Kreps, J., Langille, M.G.I., Lee, J., Ley, R., Liu, Y.-X., Loftfield, E., Lozupone, C., Maher, M., Marotz, C., Martin, B.D., McDonald, D., McIver, L.J., Melnik, A.V., Metcalf, J.L., Morgan, S.C., Morton, J.T., Naimey, A.T., Navas-Molina, J.A., Nothias, L.F., Orchanian, S.B., Pearson, T., Peoples, S.L., Petras, D., Preuss, M.L., Pruesse, E., Rasmussen, L.B., Rivers, A., Robeson, M.S., Rosenthal, P., Segata, N., Shaffer, M., Shiffer, A., Sinha, R., Song, S.J., Spear, J.R., Swafford, A.D., Thompson, L.R., Torres, P.J., Trinh, P., Tripathi, A., Turnbaugh, P.J., Ul-Hasan, S., van der Hooft, J.J.J., Vargas, F., Vázquez-Baeza, Y., Vogtmann, E., von Hippel, M., Walters, W., Wan, Y., Wang, M., Warren, J., Weber, K.C., Williamson, C.H.D., Willis, A.D., Xu, Z.Z., Zaneveld, J.R., Zhang, Y., Zhu, Q., Knight, R., Caporaso, J.G., 2019. Reproducible, interactive, scalable and extensible microbiome data science using QIIME 2. Nat Biotechnol 37, 852–857. https://doi.org/10.1038/s41587-019-0209-9

Boyle, J.F., Chiverrell, R.C., Schillereff, D.N., 2015. Approaches to water content correction and calibration for μXRF core scanning: comparing x-ray scatter with simple regression of elemental concentrations, in: Rothwell, R.G., Croudace, I.W. (Eds.), Developments in Palaeoenvironmental Research: Micro-XRF Studies of Sediment Cores. Springer, Dordrecht.

Bragazza, L., Buttler, A., Habermacher, J., Brancaleoni, L., Gerdol, R., Fritze, H., Hanajík, P., Laiho, R., Johnson, D., 2012. High nitrogen deposition alters the decomposition of bog plant litter and reduces carbon accumulation. Glob Change Biol 18, 1163–1172. https://doi.org/10.1111/j.1365-2486.2011.02585.x

Bragazza, L., Freeman, C., Jones, T., Rydin, H., Limpens, J., Fenner, N., Ellis, T., Gerdol, R., Hajek, M., Hajek, T., Iacumin, P., Kutnar, L., Tahvanainen, T., Toberman, H., 2006. Atmospheric nitrogen deposition promotes carbon loss from peat bogs. Proceedings of the National Academy of Sciences 103, 19386–19389. https://doi.org/10.1073/pnas.0606629104

Bragazza, L., Tahvanainen, T., Kutnar, L., Rydin, H., Limpens, J., Hajek, M., Grosvernier, P., Hajek, T., Hajkova, P., Hansen, I., Iacumin, P., Gerdol, R., 2004. Nutritional constraints in ombrotrophic Sphagnum plants under increasing atmospheric nitrogen deposition in Europe. New Phytol 163, 609–616. https://doi.org/10.1111/j.1469-8137.2004.01154.x

Brännvall, M., Bindler, R., Emteryd, O., Renberg, I., 2001. Four thousand years of atmospheric lead pollution in northern Europe : a summary from Swedish lake sediments. Journal of Paleolimnology 25, 421–435.

Bubier, J.L., Moore, T.R., Bledzki, L.A., 2007. Effects of nutrient addition on vegetation and carbon cycling in an ombrotrophic bog. Global Change Biology 13, 1168–1186. https://doi.org/10.1111/j.1365-2486.2007.01346.x

Bugg, T.D., Ahmad, M., Hardiman, E.M., Singh, R., 2011. The emerging role for bacteria in lignin degradation and bio-product formation. Current Opinion in Biotechnology, Energy biotechnology – Environmental biotechnology 22, 394–400. https://doi.org/10.1016/j.copbio.2010.10.009

Callahan, B.J., McMurdie, P.J., Rosen, M.J., Han, A.W., Johnson, A.J.A., Holmes, S.P., 2016. DADA2: High-resolution sample inference from Illumina amplicon data. Nat Methods 13, 581–583. https://doi.org/10.1038/nmeth.3869

Čapek, P., Manzoni, S., Kaštovská, E., Wild, B., Diáková, K., Bárta, J., Schnecker, J., Biasi, C., Martikainen, P.J., Alves, R.J.E., Guggenberger, G., Gentsch, N., Hugelius, G., Palmtag, J., Mikutta, R., Shibistova, O., Urich, T., Schleper, C., Richter, A., Šantrůčková, H., 2018. A plant–microbe interaction framework explaining nutrient effects on primary production. Nat Ecol Evol 2, 1588–1596. https://doi.org/10.1038/s41559-018-0662-8

Caporaso, J.G., Lauber, C.L., Walters, W.A., Berg-Lyons, D., Lozupone, C.A., Turnbaugh, P.J., Fierer, N., Knight, R., 2011. Global patterns of 16S rRNA diversity at a depth of millions of sequences per sample. Proceedings of the National Academy of Sciences 108, 4516–4522. https://doi.org/10.1073/pnas.1000080107

Chapman, S.J., Campbell, C.D., Fraser, A.R., Puri, G., 2001. FTIR spectroscopy of peat in and bordering Scots pine woodland: relationship with chemical and biological properties. Soil Biology and Biochemistry 33, 1193–1200. https://doi.org/10.1016/S0038-0717(01)00023-2

Charman, D.J., Beilman, D.W., Blaauw, M., Booth, R.K., Brewer, S., Chambers, F.M., Christen, J.A., Gallego-Sala, A., Harrison, S.P., Hughes, P.D.M., Jackson, S.T., Korhola, A., Mauquoy, D., Mitchell, F.J.G., Prentice, I.C., Linden, M. van der, Vleeschouwer, F.D., Yu, Z.C., Alm, J., Bauer, I.E., Corish, Y.M.C., Garneau, M., Hohl, V., Huang, Y., Karofeld, E., Roux, G.L., Loisel, J., Moschen, R., Nichols, J.E., Nieminen, T.M., MacDonald, G.M., Phadtare, N.R., Rausch, N., Sillasoo, Ü., Swindles, G.T., Tuittila, E.-S., Ukonmaanaho, L., Väliranta, M., Bellen, S. van, Geel, B. van, Vitt, D.H., Zhao, Y., 2013. Climate-related changes in peatland carbon accumulation during the last millennium. Biogeosciences 10, 929–944. https://doi.org/10.5194/bg-10-929-2013

Clymo, R.S., 1984. The Limits to Peat Bog Growth. Philosophical Transactions of the Royal Society B: Biological Sciences 303, 605–654. https://doi.org/10.1098/rstb.1984.0002

Clymo, R.S., Bryant, C.L., 2008. Diffusion and mass flow of dissolved carbon dioxide, methane, and dissolved organic carbon in a 7-m deep raised peat bog. Geochimica et Cosmochimica Acta 72, 2048–2066. https://doi.org/10.1016/j.gca.2008.01.032

Cocozza, C., D'Orazio, V., Miano, T.M., Shotyk, W., 2003. Characterization of solid and aqueous phases of a peat bog profile using molecular fluorescence spectroscopy, ESR and FT-IR, and comparison with physical properties. Organic Geochemistry 34, 49–60. https://doi.org/10.1016/S0146-6380(02)00208-5

Concheri, G., Stevanato, P., Zaccone, C., Shotyk, W., D'Orazio, V., Miano, T., Piffanelli, P., Rizzi, V., Ferrandi, C., Squartini, A., 2017. Rapid peat accumulation favours the occurrence of both fen and bog microbial communities within a Mediterranean, free-floating peat island. Sci Rep 7, 8511. https://doi.org/10.1038/s41598-017-08662-y

Coward, E.K., Ohno, T., Sparks, D.L., 2019. Direct Evidence for Temporal Molecular Fractionation of Dissolved Organic Matter at the Iron Oxyhydroxide Interface. Environ. Sci. Technol. 53, 642–650. https://doi.org/10.1021/acs.est.8b04687

Dedysh, S.N., Pankratov, T.A., Belova, S.E., Kulichevskaya, I.S., Liesack, W., 2006. Phylogenetic Analysis and In Situ Identification of Bacteria Community Composition in an Acidic Sphagnum Peat Bog. Applied and Environmental Microbiology 72, 2110–2117. https://doi.org/10.1128/AEM.72.3.2110-2117.2006

Dom, S.P., Ikenaga, M., Lau, S.Y.L., Radu, S., Midot, F., Yap, M.L., Chin, M.-Y., Lo, M.L., Jee, M.S., Maie, N., Melling, L., 2021. Linking prokaryotic community composition to carbon biogeochemical cycling across a tropical peat dome in Sarawak, Malaysia. Sci Rep 11, 6416. https://doi.org/10.1038/s41598-021-81865-6

Doskočil, L., Enev, V., Pekař, M., Wasserbauer, J., 2016. The spectrometric characterization of lipids extracted from lignite samples from various coal basins. Organic Geochemistry 95, 34–40. https://doi.org/10.1016/j.orggeochem.2016.02.008

Dunnington, D.W., Libera, N., Kurek, J., Spooner, I.S., Gagnon, G.A., 2022. tidypaleo: Visualizing Paleoenvironmental Archives Using ggplot2. Journal of Statistical Software 101, 1–20. https://doi.org/10.18637/jss.v101.i07

Emsens, W.-J., Van Diggelen, R., Aggenbach, C.J.S., Cajthaml, T., Frouz, J., Klimkowska, A., Kotowski, W., Kozub, L., Liczner, Y., Seeber, E., Silvennoinen, H., Tanneberger, F., Vicena, J., Wilk, M., Verbruggen, E., 2020. Recovery of fen peatland microbiomes and predicted functional profiles after rewetting. The ISME Journal 14, 1701–1712. https://doi.org/10.1038/s41396-020-0639-x

Fenner, N., Freeman, C., 2011. Drought-induced carbon loss in peatlands. Nature Geosci 4, 895–900. https://doi.org/10.1038/ngeo1323

Fritz, C., van Dijk, G., Smolders, A.J.P., Pancotto, V.A., Elzenga, T.J.T.M., Roelofs, J.G.M., Grootjans, A.P., 2012. Nutrient additions in pristine Patagonian Sphagnum bog vegetation: can phosphorus addition alleviate (the effects of) increased nitrogen loads: Nutrient additions in pristine Patagonian Sphagnum bog vegetation. Plant Biology 14, 491–499. https://doi.org/10.1111/j.1438-8677.2011.00527.x

Goldstein, A., Turner, W.R., Spawn, S.A., Anderson-Teixeira, K.J., Cook-Patton, S., Fargione, J., Gibbs, H.K., Griscom, B., Hewson, J.H., Howard, J.F., Ledezma, J.C., Page, S., Koh, L.P., Rockström, J., Sanderman, J., Hole, D.G., 2020. Protecting irrecoverable carbon in Earth's ecosystems. Nat. Clim. Chang. 10, 287–295. https://doi.org/10.1038/s41558-020-0738-8

Gorham, E., 1991. Northern Peatlands: Role in the Carbon Cycle and Probable Responses to Climatic Warming. Ecological Applications 1, 182–195. https://doi.org/10.2307/1941811

Gorham, E., Lehman, C., Dyke, A., Clymo, D., Janssens, J., 2012. Long-term carbon sequestration in North American peatlands. Quaternary Science Reviews 58, 77–82. https://doi.org/10.1016/j.quascirev.2012.09.018

Gunnarsson, U., Granberg, G., Nilsson, M., 2004. Growth, production and interspecific competition in Sphagnum: effects of temperature, nitrogen and sulphur treatments on a boreal mire. New Phytologist 163, 349–359. https://doi.org/10.1111/j.1469-8137.2004.01108.x

Hájek, T., Ballance, S., Limpens, J., Zijlstra, M., Verhoeven, J.T.A., 2011. Cell-wall polysaccharides play an important role in decay resistance of Sphagnum and actively depressed decomposition in vitro. Biogeochemistry 103, 45–57. https://doi.org/10.1007/s10533-010-9444-3

Jääskeläinen, A.S., Sun, Y., Argyropoulos, D.S., Tamminen, T., Hortling, B., 2003. The effect of isolation method on the chemical structure of residual lignin. Wood Science and Technology 37, 91–102. https://doi.org/10.1007/s00226-003-0163-y

Jaatinen, K., Fritze, H., Laine, J., Laiho, R., 2007. Effects of short- and long-term water-level drawdown on the populations and activity of aerobic decomposers in a boreal peatland. Global Change Biology 13, 491–510. https://doi.org/10.1111/j.1365-2486.2006.01312.x

Jehlička, J., Edwards, H.G.M., 2008. Raman spectroscopy as a tool for the non-destructive identification of organic minerals in the geological record. Organic Geochemistry 39, 371–386. https://doi.org/10.1016/j.orggeochem.2008.01.005

Jiang, L., Song, Y., Sun, L., Ma, X., Wang, X., Song, C., Hou, A., Wang, L., 2021. Distribution of carbon and nitrogen cycle microbes along permafrost peatland profile in Northeast China. Environmental Progress & Sustainable Energy 40, e13707. https://doi.org/10.1002/ep.13707

Keller, J.K., Bauers, A.K., Bridgham, S.D., Kellogg, L.E., Iversen, C.M., 2006. Nutrient control of microbial carbon cycling along an ombrotrophic-minerotrophic peatland gradient. Journal of Geophysical Research 111. https://doi.org/10.1029/2005JG000152

Kolton, M., Weston, D.J., Mayali, X., Weber, P.K., McFarlane, K.J., Pett-Ridge, J., Somoza, M.M., Lietard, J., Glass, J.B., Lilleskov, E.A., Shaw, A.J., Tringe, S., Hanson, P.J., Kostka, J.E., 2022. Defining the Sphagnum Core Microbiome across the North American Continent Reveals a Central Role for Diazotrophic Methanotrophs in the Nitrogen and

Carbon Cycles of Boreal Peatland Ecosystems. mBio 13, e03714-21. https://doi.org/10.1128/mbio.03714-21

Kylander, M.E., Bindler, R., Cortizas, A.M., Gallagher, K., Mörth, C.-M., Rauch, S., 2013. A novel geochemical approach to paleorecords of dust deposition and effective humidity: 8500 years of peat accumulation at Store Mosse (the “Great Bog”), Sweden. Quaternary Science Reviews 69, 69–82. https://doi.org/10.1016/j.quascirev.2013.02.010

Kylander, M.E., Martínez-Cortizas, A., Bindler, R., Greenwood, S.L., Mörth, C.-M., Rauch, S., 2016. Potentials and problems of building detailed dust records using peat archives: An example from Store Mosse (the “Great Bog”), Sweden. Geochimica et Cosmochimica Acta 190, 156–174. https://doi.org/10.1016/j.gca.2016.06.028

Kylander, M.E., Martínez-Cortizas, A., Bindler, R., Kaal, J., Sjöström, J.K., Hansson, S.V., Silva-Sánchez, N., Greenwood, S.L., Gallagher, K., Rydberg, J., Mörth, C.-M., Rauch, S., 2018. Mineral dust as a driver of carbon accumulation in northern latitudes. Sci Rep 8, 6876. https://doi.org/10.1038/s41598-018-25162-9

Larsson, A., Segerström, U., Laudon, H., Nilsson, M.B., 2017. Holocene carbon and nitrogen accumulation rates in a boreal oligotrophic fen. The Holocene 27, 811–821. https://doi.org/10.1177/0959683616675936

Li, W., Luo, M., Shi, R., Feng, D., Yang, Z., Chen, H., Hu, B., 2022. Variations in bacterial and archaeal community structure and diversity along the soil profiles of a peatland in Southwest China. Environ Sci Pollut Res 29, 2276–2286. https://doi.org/10.1007/s11356-021-15774-6

Lin, X., Tfaily, M.M., Green, S.J., Steinweg, J.M., Chanton, P., Imvittaya, A., Chanton, J.P., Cooper, W., Schadt, C., Kostka, J.E., 2014a. Microbial Metabolic Potential for Carbon Degradation and Nutrient (Nitrogen and Phosphorus) Acquisition in an Ombrotrophic Peatland. Appl. Environ. Microbiol. 80, 3531–3540. https://doi.org/10.1128/AEM.00206-14

Lin, X., Tfaily, M.M., Steinweg, J.M., Chanton, P., Esson, K., Yang, Z.K., Chanton, J.P., Cooper, W., Schadt, C.W., Kostka, J.E., 2014b. Microbial Community Stratification Linked to Utilization of Carbohydrates and Phosphorus Limitation in a Boreal Peatland at Marcell Experimental Forest, Minnesota, USA. Applied and Environmental Microbiology 80, 3518–3530. https://doi.org/10.1128/AEM.00205-14

Liu, H., Gu, Y., Ge, J., Yu, Z., Xu, X., Zhang, Z., Cheng, S., Xie, S., 2022. The response of the Dajiuhu Peatland ecosystem to hydrological variations: Implications for carbon sequestration and peatlands conservation. Journal of Hydrology 612, 128307. https://doi.org/10.1016/j.jhydrol.2022.128307

Loisel, J., Gallego-Sala, A., 2022. Ecological resilience of restored peatlands to climate change. Commun Earth Environ 3, 1–8. https://doi.org/10.1038/s43247-022-00547-x

Loisel, J., van Bellen, S., Pelletier, L., Talbot, J., Hugelius, G., Karran, D., Yu, Z., Nichols, J., Holmquist, J., 2017. Insights and issues with estimating northern peatland carbon stocks and fluxes since the Last Glacial Maximum. Earth-Science Reviews 165, 59–80. https://doi.org/10.1016/j.earscirev.2016.12.001

Loisel, J., Yu, Z., Beilman, D.W., Camill, P., Alm, J., Amesbury, M.J., Anderson, D., Andersson, S., Bochicchio, C., Barber, K., Belyea, L.R., Bunbury, J., Chambers, F.M., Charman, D.J., De Vleeschouwer, F., Fiałkiewicz-Kozieł, B., Finkelstein, S.A., Gałka, M., Garneau, M., Hammarlund, D., Hinchcliffe, W., Holmquist, J., Hughes, P., Jones, M.C., Klein, E.S., Kokfelt, U., Korhola, A., Kuhry, P., Lamarre, A., Lamentowicz, M., Large, D., Lavoie, M., MacDonald, G., Magnan, G., Mäkilä, M., Mallon, G., Mathijssen, P., Mauquoy, D., McCarroll, J., Moore, T.R., Nichols, J., O'Reilly, B., Oksanen, P., Packalen, M., Peteet, D., Richard, P.J., Robinson, S., Ronkainen, T., Rundgren, M., Sannel, A.B.K., Tarnocai, C., Thom, T., Tuittila, E.-S., Turetsky, M., Väliranta, M., van der Linden, M., van Geel, B., van Bellen, S., Vitt, D., Zhao, Y., Zhou, W., 2014. A database and synthesis of northern peatland soil properties and Holocene carbon and nitrogen accumulation. The Holocene 24, 1028–1042. https://doi.org/10.1177/0959683614538073

Lu, F., Wu, J., Yi, B., Xu, Z., Wang, M., Sundberg, S., Bu, Z.-J., 2022. Long-Term Phosphorus Addition Strongly Weakens the Carbon Sink Function of a Temperate Peatland. Ecosystems. https://doi.org/10.1007/s10021-022-00754-9

Malmer, N., Albinsson, C., Svensson, B.M., Wallén, B., 2003. Interferences between Sphagnum and vascular plants: effects on plant community structure and peat formation. Oikos 100, 469–482. https://doi.org/10.1034/j.1600-0706.2003.12170.x

Malmer, N., Wallén, B., 2004. Input rates, decay losses and accumulation rates of carbon in bogs during the last millennium: internal processes and environmental changes. The Holocene 14, 111–117. https://doi.org/10.1191/0959683604hl693rp

Martin, M., 2011. Cutadapt removes adapter sequences from high-throughput sequencing reads. EMBnet.journal 17, 10–12. https://doi.org/10.14806/ej.17.1.200

Martínez Cortizas, A., Sjöström, J.K., Ryberg, E.E., Kylander, M.E., Kaal, J., López-Costas, O., Álvarez Fernández, N., Bindler, R., 2021. 9000 years of changes in peat organic matter composition in Store Mosse (Sweden) traced using FTIR-ATR. Boreas 50, 1161–1178. https://doi.org/10.1111/bor.12527

Martínez Cortizas, A., Traoré, M., López-Costas, O., Sjöström, J.K., Kylander, M.E., 2024. Beyond the Obvious: Exploring Peat Vibrational Spectroscopy (FTIR-ATR) Data Using Principal Components Analysis on Transposed Data Matrix (tPCA), Store Mosse Bog (Sweden), in: Núñez-Delgado, A. (Ed.), Frontier Studies in Soil Science. Springer International Publishing, Cham, pp. 217–247. https://doi.org/10.1007/978-3-031-50503-4_11

Mastný, J., Bárta, J., Kaštovská, E., Picek, T., 2021. Decomposition of peatland DOC affected by root exudates is driven by specific r and K strategic bacterial taxa. Sci Rep 11, 18677. https://doi.org/10.1038/s41598-021-97698-2

Minor, E., Stephens, B., 2008. Dissolved organic matter characteristics within the Lake Superior watershed. Organic Geochemistry 39, 1489–1501. https://doi.org/10.1016/j.orggeochem.2008.08.001

Moore, T.R., Bubier, J.L., Bledzki, L., 2007. Litter Decomposition in Temperate Peatland Ecosystems: The Effect of Substrate and Site. Ecosystems 10, 949–963. https://doi.org/10.1007/s10021-007-9064-5

Moore, T.R., Knorr, K.-H., Thompson, L., Roy, C., Bubier, J.L., 2019. The effect of long-term fertilization on peat in an ombrotrophic bog. Geoderma 343, 176–186. https://doi.org/10.1016/j.geoderma.2019.02.034

Morales, S.E., Mouser, P.J., Ward, N., Hudman, S.P., Gotelli, N.J., Ross, D.S., Lewis, T.A., 2006. Comparison of Bacterial Communities in New England Sphagnum Bogs Using Terminal Restriction Fragment Length Polymorphism (T-RFLP). Microb Ecol 52, 34–44. https://doi.org/10.1007/s00248-005-0264-2

Muthreich, F., Zimmermann, B., Birks, H.J.B., Vila-Viçosa, C.M., Seddon, A.W.R., 2020. Chemical variations in *Quercus* pollen as a tool for taxonomic identification: Implications for long-term ecological and biogeographical research. Journal of Biogeography 47, 1298–1309. https://doi.org/10.1111/jbi.13817

Nakayama, Y., Yamaguchi, H., Einaga, N., Esumi, M., 2016. Pitfalls of DNA Quantification Using DNA-Binding Fluorescent Dyes and Suggested Solutions. PLOS ONE 11, e0150528. https://doi.org/10.1371/journal.pone.0150528

Niemeyer, J., Chen, Y., Bollag, J. -M., 1992. Characterization of Humic Acids, Composts, and Peat by Diffuse Reflectance Fourier-Transform Infrared Spectroscopy. Soil Science Soc of Amer J 56, 135–140. https://doi.org/10.2136/sssaj1992.03615995005600010021x

Oksanen, A.J., Blanchet, F.G., Kindt, R., Legen-, P., Minchin, P.R., Hara, R.B.O., Simpson, G.L., Solymos, P., Stevens, M.H.H., Wagner, H., 2013. Package 'vegan.'

Pankratov, T.A., Ivanova, A.O., Dedysh, S.N., Liesack, W., 2011. Bacterial populations and environmental factors controlling cellulose degradation in an acidic Sphagnum peat. Environmental Microbiology 13, 1800–1814. https://doi.org/10.1111/j.1462-2920.2011.02491.x

Passauer, L., Struch, M., Schuldt, S., Appelt, J., Schneider, Y., Jaros, D., Rohm, H., 2012. Dynamic Moisture Sorption Characteristics of Xerogels from Water-Swellable Oligo(oxyethylene) Lignin Derivatives. ACS Appl. Mater. Interfaces 4, 5852–5862. https://doi.org/10.1021/am3015179

Pedregosa, F., Pedregosa, F., Varoquaux, G., Varoquaux, G., Org, N., Gramfort, A., Gramfort, A., Michel, V., Michel, V., Fr, L., Thirion, B., Thirion, B., Grisel, O., Grisel, O., Blondel, M., Prettenhofer, P., Prettenhofer, P., Weiss, R., Dubourg, V., Dubourg, V., Vanderplas, J., Passos, A., Tp, A., Cournapeau, D., n.d. Scikit-learn: Machine Learning in Python. MACHINE LEARNING IN PYTHON.

Potter, C., Freeman, C., Golyshin, P.N., Ackermann, G., Fenner, N., McDonald, J.E., Ehbair, A., Jones, T.G., Murphy, L.M., Creer, S., 2017. Subtle shifts in microbial communities occur alongside the release of carbon induced by drought and rewetting in contrasting peatland ecosystems. Sci Rep 7, 11314. https://doi.org/10.1038/s41598-017-11546-w

Preston, M.D., Smemo, K.A., McLaughlin, J.W., Basiliko, N., 2012. Peatland Microbial Communities and Decomposition Processes in the James Bay Lowlands, Canada. Front. Microbiol. 3. https://doi.org/10.3389/fmicb.2012.00070

Puglisi, E., Zaccone, C., Cappa, F., Cocconcelli, P.S., Shotyk, W., Trevisan, M., Miano, T.M., 2014. Changes in bacterial and archaeal community assemblages along an ombrotrophic peat bog profile. Biol Fertil Soils 50, 815–826. https://doi.org/10.1007/s00374-014-0902-2

Rana, R., Langenfeld-Heyser, R., Finkeldey, R., Polle, A., 2010. FTIR spectroscopy, chemical and histochemical characterisation of wood and lignin of five tropical timber wood species of the family of Dipterocarpaceae. Wood Sci Technol 44, 225–242. https://doi.org/10.1007/s00226-009-0281-2

Ratcliffe, J., Andersen, R., Anderson, R., Newton, A., Campbell, D., Mauquoy, D., Payne, R., 2018. Contemporary carbon fluxes do not reflect the long-term carbon balance for an Atlantic blanket bog. The Holocene 28, 140–149. https://doi.org/10.1177/0959683617715689

Ratcliffe, J.L., Lowe, D.J., Schipper, L.A., Gehrels, M.J., French, A.D., Campbell, D.I., 2020. Rapid carbon accumulation in a peatland following Late Holocene tephra deposition, New Zealand. Quaternary Science Reviews 246, 106505. https://doi.org/10.1016/j.quascirev.2020.106505

Richy, E., Cabello-Yeves, P.J., Hernandes-Coutinho, F., Rodriguez-Valera, F., González-Álvarez, I., Gandois, L., Rigal, F., Lauga, B., 2024. How microbial communities shape peatland carbon dynamics: New insights and implications. Soil Biology and Biochemistry 191, 109345. https://doi.org/10.1016/j.soilbio.2024.109345

Robroek, B.J.M., Devilee, G., Telgenkamp, Y., Härlin, C., Steele, M.N., Barel, J.M., Lamers, L.P.M., 2024. More is not always better: peat moss mixtures slightly enhance peatland stability. Proceedings of the Royal Society B: Biological Sciences 291, 20232622. https://doi.org/10.1098/rspb.2023.2622

Romanowicz, K.J., 2013. Plant-mediated effects on microbial diversity in mesocosms of an oligotrophic bog (M.S.). Michigan Technological University, United States -- Michigan.

Roth, S.W., Griffiths, N.A., Kolka, R.K., Oleheiser, K.C., Carrell, A.A., Klingeman, D.M., Seibert, A., Chanton, J.P., Hanson, P.J., Schadt, C.W., 2023. Elevated temperature alters microbial communities, but not decomposition rates, during 3 years of in situ peat decomposition. mSystems 8, e00337-23. https://doi.org/10.1128/msystems.00337-23

Roulet, N.T., Ash, R., Quinton, W., Moore, T., 1993. Methane flux from drained northern peatlands: Effect of a persistent water table lowering on flux. Global Biogeochemical Cycles 7, 749–769. https://doi.org/10.1029/93GB01931

Russell, F.E., Boyle, J.F., Chiverrell, R.C., 2019. NIRS quantification of lake sediment composition by multiple regression using end-member spectra. J Paleolimnol 62, 73–88. https://doi.org/10.1007/s10933-019-00076-2

Ryberg, E.E., Väliranta, M., Martinez-Cortizas, A., Ehrlén, J., Sjöström, J.K., Kylander, M.E., 2022. Postglacial peatland vegetation succession in Store Mosse bog, south-central Sweden: An exploration of factors driving species change. Boreas 51, 651–666. https://doi.org/10.1111/bor.12580

Rydin, H., Jeglum, J., 2013. The Biology of Peatlands, 2nd Edition. ed. Oxford University Press, Oxford, UK.

Scheffer, R.A., Van Logtestijn, R.S.P., Verhoeven, J.T.A., 2001. Decomposition of Carex and Sphagnum litter in two mesotrophic fens differing in dominant plant species. Oikos 92, 44–54. https://doi.org/10.1034/j.1600-0706.2001.920106.x

Schillereff, D.N., Chiverrell, R.C., Sjöström, J.K., Kylander, M.E., Boyle, J.F., Davies, J.A.C., Toberman, H., Tipping, E., 2021. Phosphorus supply affects long-term carbon accumulation in mid-latitude ombrotrophic peatlands. Commun Earth Environ 2, 241. https://doi.org/10.1038/s43247-021-00316-2

Senesi, N., Miano, T.M., Provenzano, M.R., Brunetti, G., 1989. Spectroscopic and compositional comparative characterization of I.H.S.S. reference and standard fulvic and humic acids of various origin. Science of The Total Environment 81–82, 143–156. https://doi.org/10.1016/0048-9697(89)90120-4

Seward, J., Carson, M.A., Lamit, L.J., Basiliko, N., Yavitt, J.B., Lilleskov, E., Schadt, C.W., Smith, D.S., Mclaughlin, J., Mykytczuk, N., Willims-Johnson, S., Roulet, N., Moore, T., Harris, L., Bräuer, S., 2020. Peatland Microbial Community Composition Is Driven by a Natural Climate Gradient. Microb Ecol 80, 593–602. https://doi.org/10.1007/s00248-020-01510-z

Sjöström, J.K., Bindler, R., Martínez Cortizas, A., Björck, S., Hansson, S.V., Karlsson, A., Ellerton, D.T., Kylander, M.E., 2022. Late Holocene peat paleodust deposition in south-western Sweden - exploring geochemical properties, local mineral sources and regional aeolian activity. Chemical Geology 602, 120881. https://doi.org/10.1016/j.chemgeo.2022.120881

Sjöström, J.K., Martínez Cortizas, A., Hansson, S.V., Silva Sánchez, N., Bindler, R., Rydberg, J., Mörth, C.-M., Ryberg, E.E., Kylander, M.E., 2020. Paleodust deposition and peat accumulation rates – Bog size matters. Chemical Geology 554, 119795. https://doi.org/10.1016/j.chemgeo.2020.119795

St. James, A.R., Lin, J., Richardson, R.E., 2021. Relationship Between Peat Type and Microbial Ecology in Sphagnum-Containing Peatlands of the Adirondack Mountains, NY, USA. Microb Ecol 82, 429–441. https://doi.org/10.1007/s00248-020-01651-1

Svensson, G., 1988. Bog development and environmental conditions as shown by the stratigraphy of Store Mosse mire in southern Sweden. Boreas 17, 89–111. https://doi.org/10.1111/j.1502-3885.1988.tb00126.x

Tsitko, I., Lusa, M., Lehto, J., Parviainen, L., Ikonen, A.T.K., Lahdenperä, A.-M., Bomberg, M., 2014. The Variation of Microbial Communities in a Depth Profile of an Acidic, Nutrient-Poor Boreal Bog in Southwestern Finland. Open Journal of Ecology 04, 832. https://doi.org/10.4236/oje.2014.413071

Tveit, A., Schwacke, R., Svenning, M.M., Urich, T., 2013. Organic carbon transformations in high-Arctic peat soils: key functions and microorganisms. The ISME Journal 7, 299–311. https://doi.org/10.1038/ismej.2012.99

van Breemen, N., 1995. How *Sphagnum* bogs down other plants. Trends in Ecology & Evolution 10, 270–275. https://doi.org/10.1016/0169-5347(95)90007-1

van Ravenhorst, L., 2022. Peatland restoration: A mossy affair? : The similarities of the vegetation communitiesbetween restored bogs and natural bogs.

Verhoeven, J.T.A., Liefveld, W.M., 1997. The ecological significance of organochemical compounds in *Sphagnum*. Acta Botanica Neerlandica 46, 117–130. https://doi.org/10.1111/plb.1997.46.2.117

Wang, H.-Y., Yu, Z.-G., Zhou, F.-W., Hernandez, J.-C., Grandjean, A., Biester, H., Xiao, K.-Q., Knorr, K.-H., 2024. Microbial communities and functions are structured by vertical geochemical zones in a northern peatland. Science of The Total Environment 950, 175273. https://doi.org/10.1016/j.scitotenv.2024.175273

Wang, M., Moore, T.R., Talbot, J., Riley, J.L., 2015. The stoichiometry of carbon and nutrients in peat formation. Global Biogeochemical Cycles 29, 113–121. https://doi.org/10.1002/2014GB005000

Wang, M., Tian, J., Bu, Z., Lamit, L.J., Chen, H., Zhu, Q., Peng, C., 2019. Structural and functional differentiation of the microbial community in the surface and subsurface peat of two minerotrophic fens in China. Plant Soil 437, 21–40. https://doi.org/10.1007/s11104-019-03962-w

Wickham, H., 2016. ggplot2.

Wood, J.R., Burge, O.R., Bolstridge, N., Bonner, K., Clarkson, B., Cole, T.L., Davis, C., Fergus, A., King, P., McKeown, M.M., Morse, C., Richardson, S.J., Robertson, H., Wilmshurst, J.M., 2021. Vertical distribution of prokaryotes communities and predicted metabolic pathways in New Zealand wetlands, and potential for environmental DNA indicators of wetland condition. PLOS ONE 16, e0243363. https://doi.org/10.1371/journal.pone.0243363

Yamamuro, M., Kayanne, H., 1995. Rapid direct determination of organic carbon and nitrogen in carbonate-bearing sediments with a Yanaco MT-5 CHN analyzer. Limnology and Oceanography 40, 1001–1005. https://doi.org/10.4319/lo.1995.40.5.1001

Zaccone, C., Miano, T.M., Shotyk, W., 2007. Qualitative comparison between raw peat and related humic acids in an ombrotrophic bog profile. Organic Geochemistry 38, 151–160. https://doi.org/10.1016/j.orggeochem.2006.06.023

Zhang, Y., Wang, J., Xue, S., Wu, J., Chang, L., Li, Z., 2016. Kinetic study on changes in methyl and methylene groups during low-temperature oxidation of coal via in-situ FTIR. International Journal of Coal Geology 155–164. http://dx.doi.org/10.1016/j.coal.2016.01.002

## Supplemental material

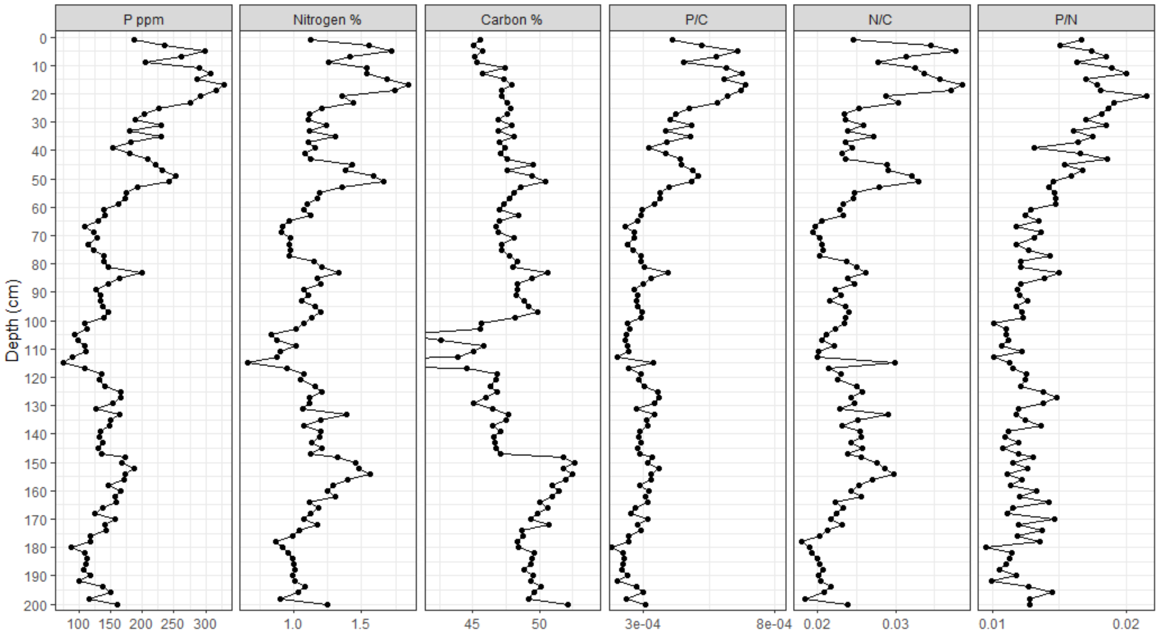

**Figure S1.** Biogeochemical and stoichiometric profiles for Store Mosse. We plot ratios inverse to the convention to highlight periods of higher relative nutrient content.

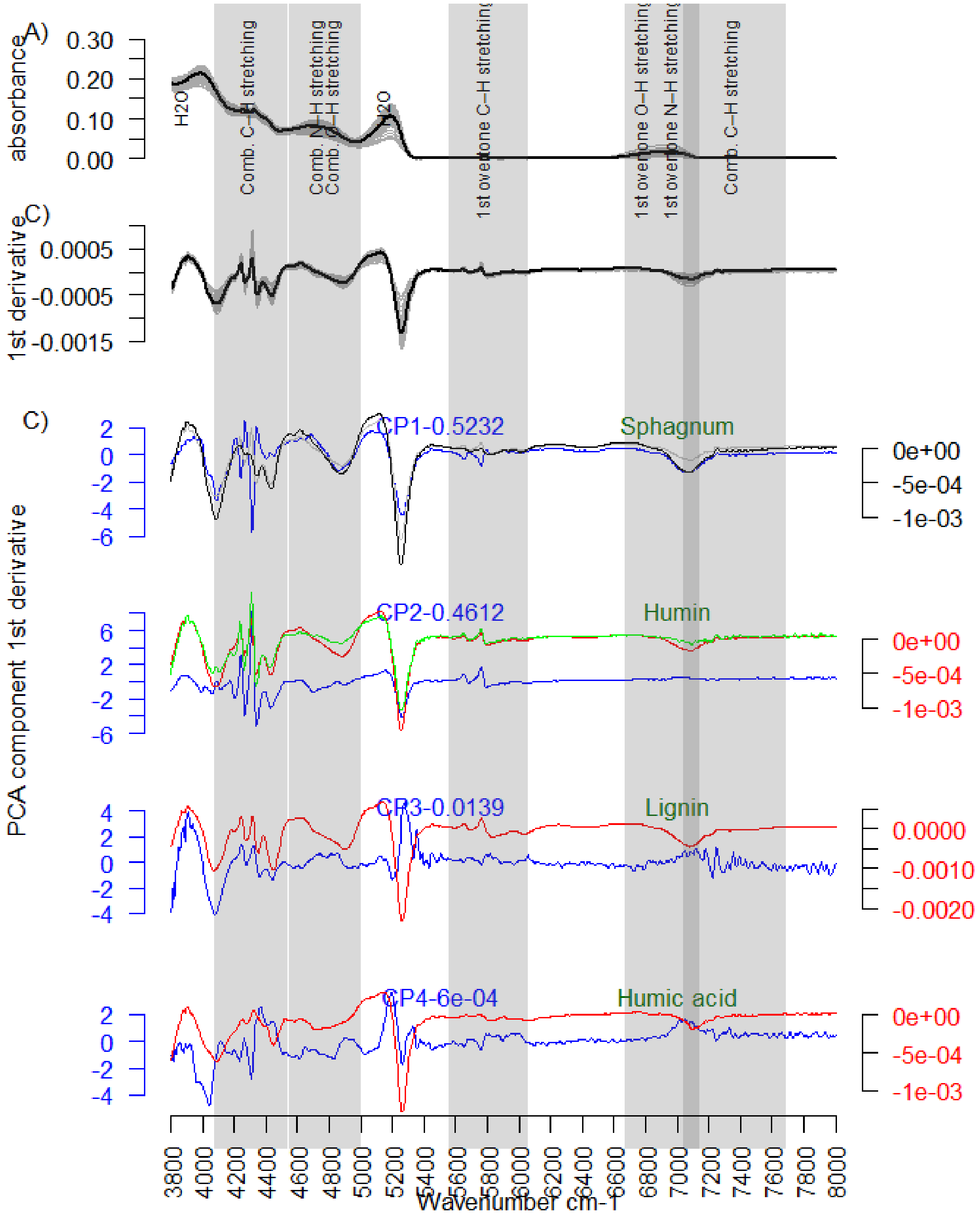

**Figure S2.** A) Cloud of the NIR baseline corrected absorbance spectra. B) First derivatives for all Store Mosse samples (grey) and the average $1^{st}$ derivative (Black) for all samples. C) First-derivative NIR spectra for the four modelled principal components and end members tested from the University of Liverpool NIRS library (Table 2). Grey shading denote major organic and water NIRS bands.

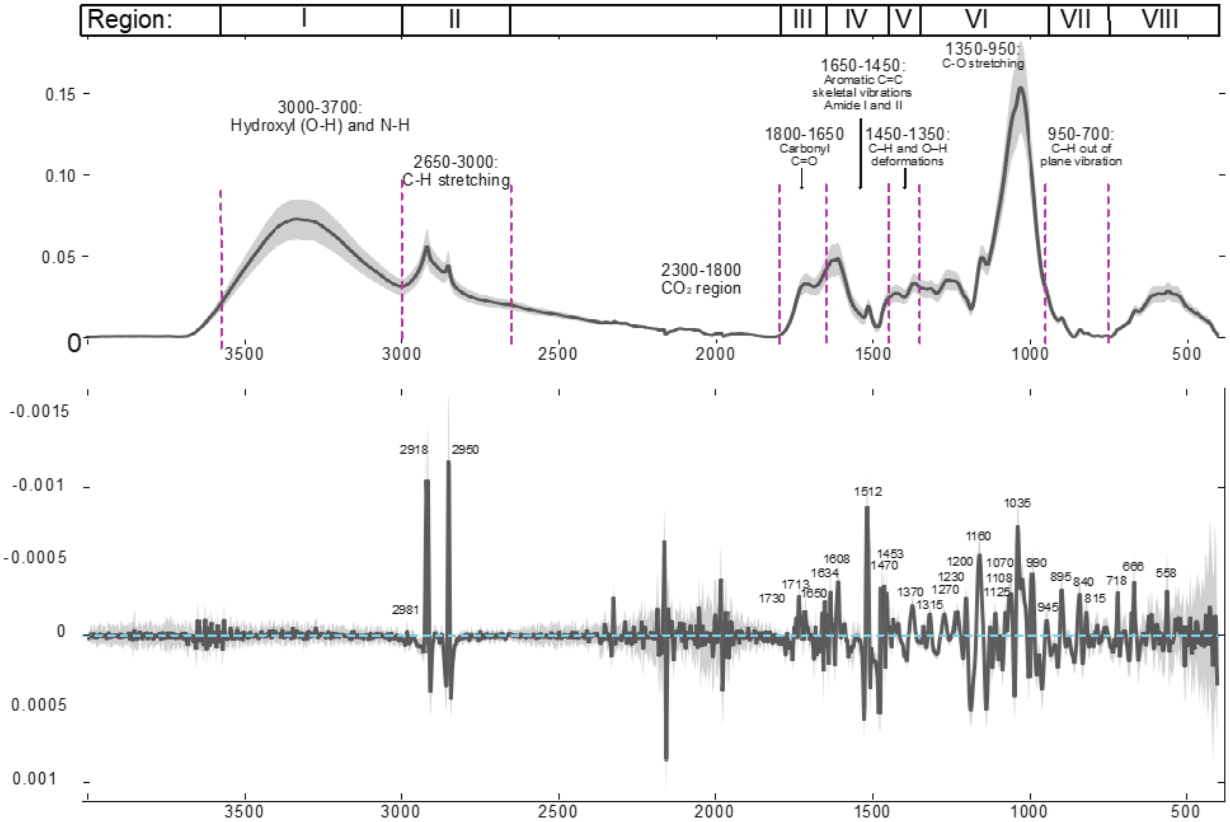

**Figure S3. A)** Average and standard deviation of all FTIR-ATR analysed samples. The areas where the standard deviation is greater represents areas with larger differences between samples. The division of the mid-infrared spectra into eight (I-VIII) regions is presented in the top row, with the corresponding vibrations of each region. These represent the main functional groups and their relative variation in absorbance (Table S2). The region at 2300-1800 cm$^{-1}$ may record background differences in $CO_2$ during the measurements so will not be considered here.

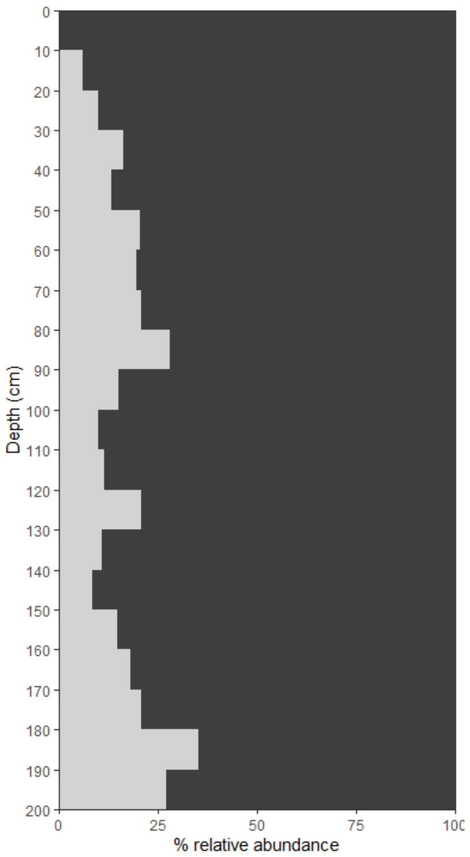

**Figure S4.** Downcore abundance of total bacteria relative to archaea

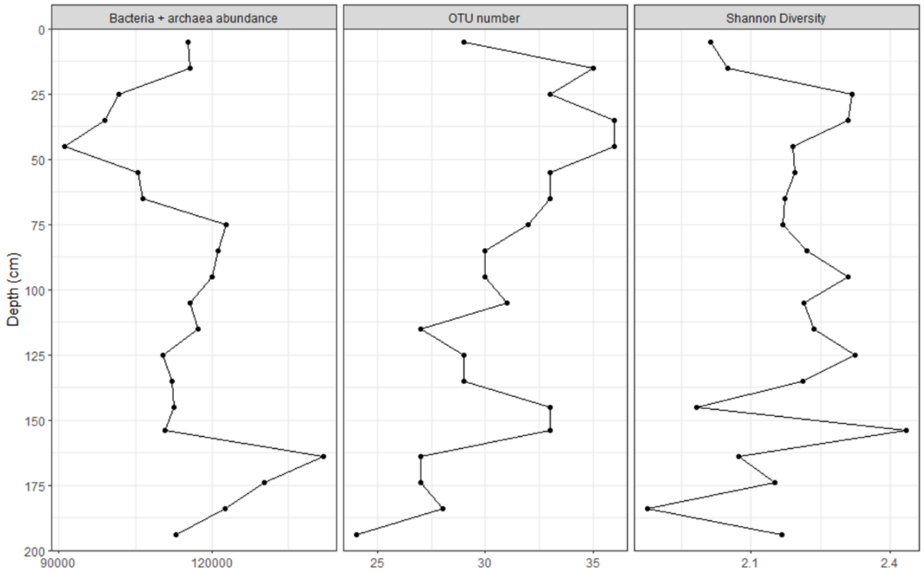

**Figure S5.** Alpha diversity and OTU profiles for the phylum level.

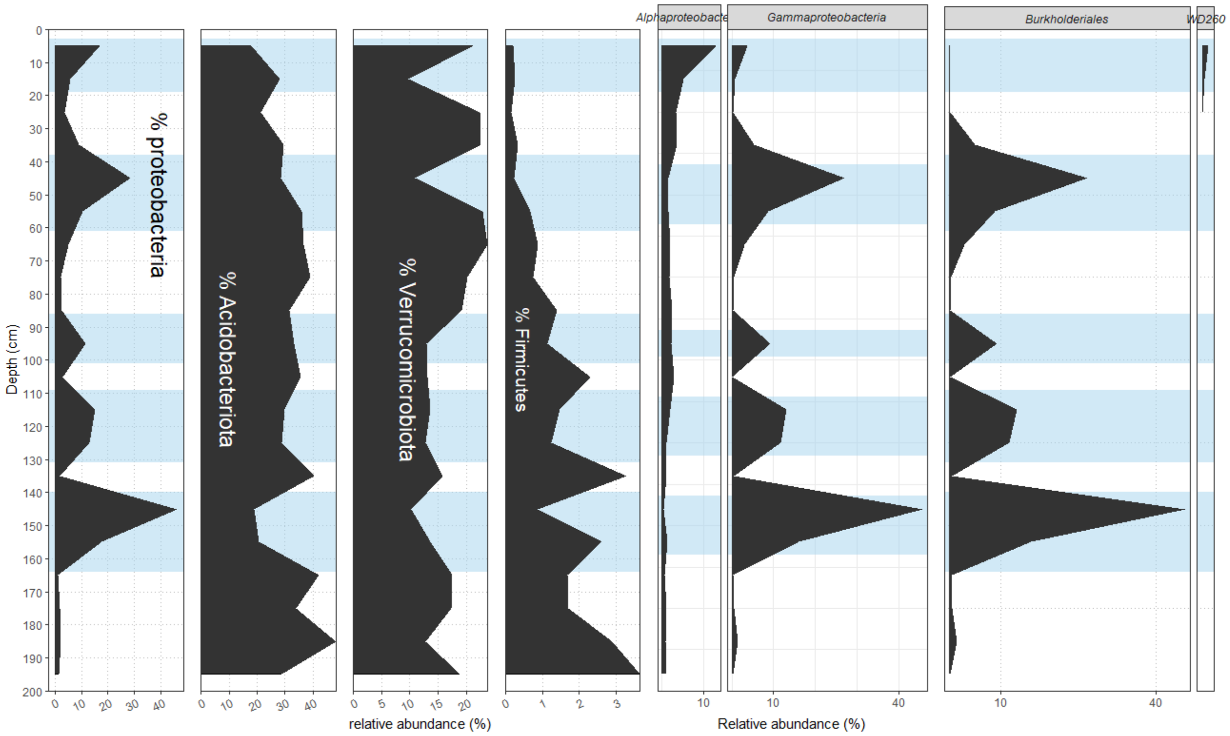

**Figure S6.** Abundance plots of four key bacterial phyla. *Alpha* and *Gammaproteobacteria* and *Burkholderiales* and *WD260* are the main Classes and Orders, respectively, within the *Proteobacteria* phylum at Store Mosse. Blue zones represent intervals of peaks in % proteobacteria and troughs in the other major phyla.

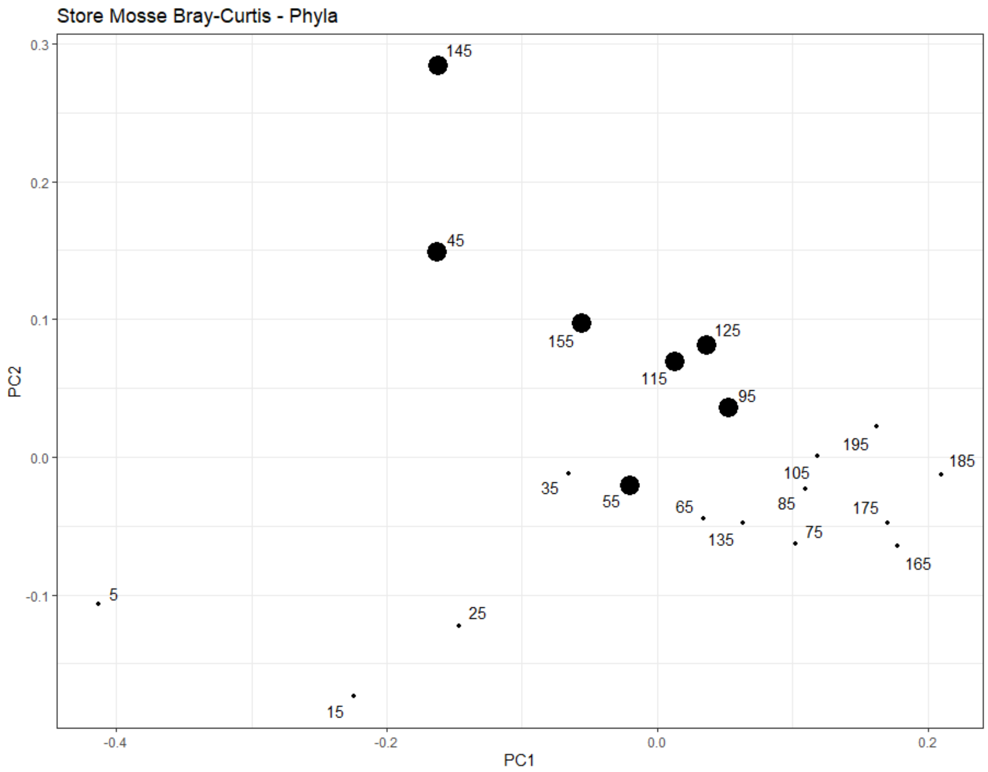

**Figure S7.** Bray-Curtis ordination. Labels are sample depths in centimetres. Large dots denote samples with high *Proteobacteria* abundance, showing those depths differ in microbial community composition in parallel with proxies of nutrient input and decomposition.

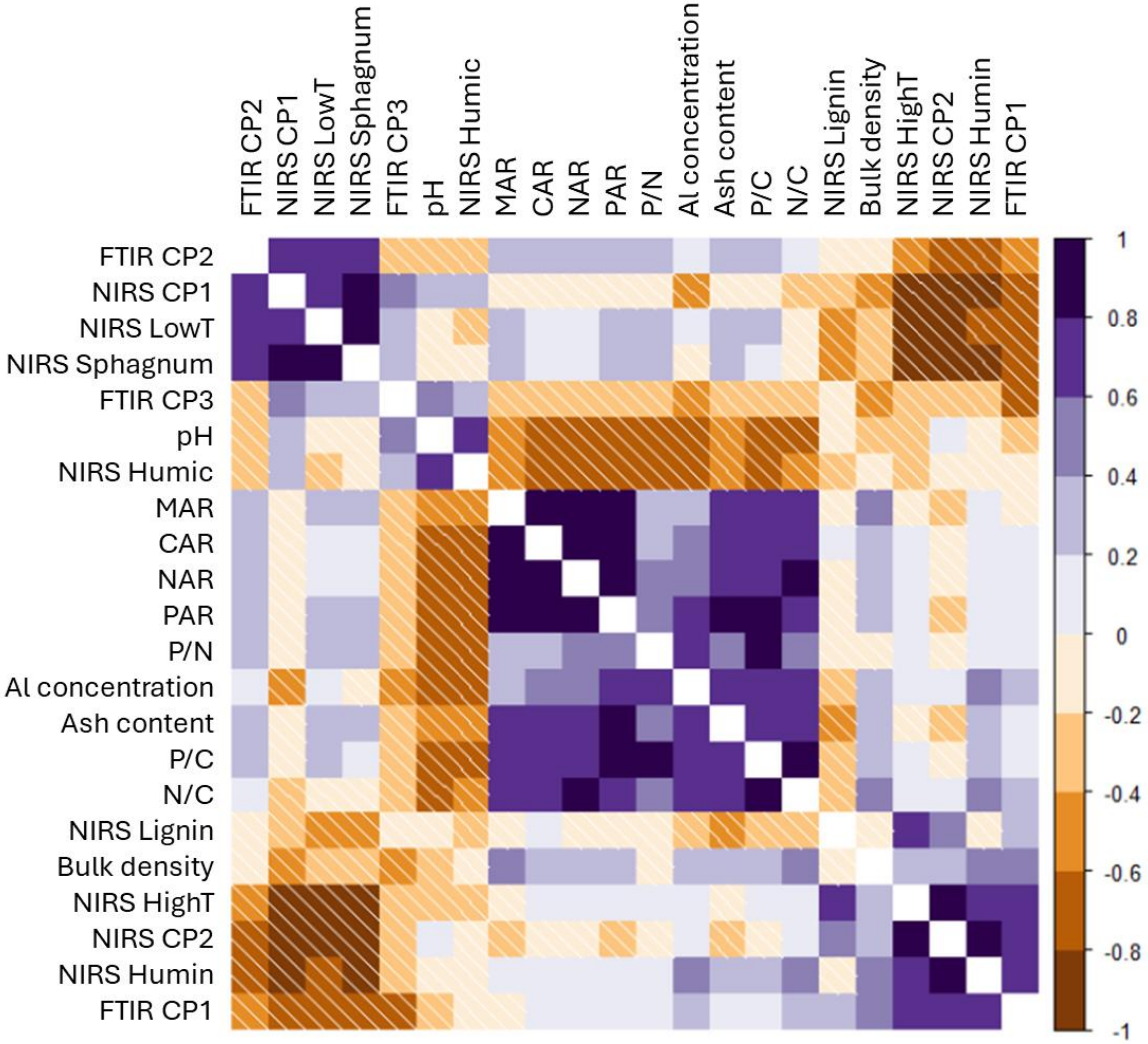

**Figure S8.** Correlation matrix. MAR, CAR, NAR and PAR represent Mass, Carbon, Nitrogen and Phosphorus accumulation rates, respectively.

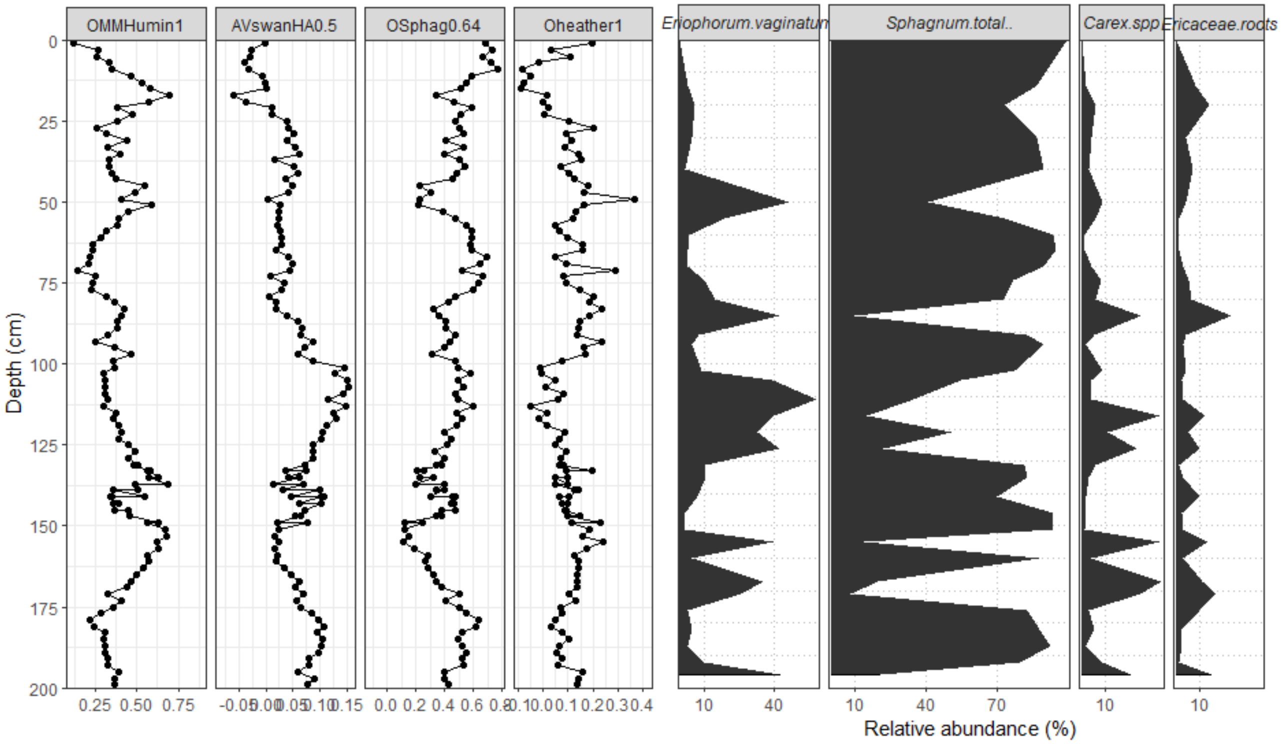

**Figure S9.** NIRS-derived litter composition compared to plant macrofossil data of Ryberg et al. 2022 from a core in the same area of Store Mosse. NIRS-Sphagnum peaks generally correspond with macrofossil counts, although there is a depth offset at 80 – 120-cm, which is reflected in the bulk density curves.

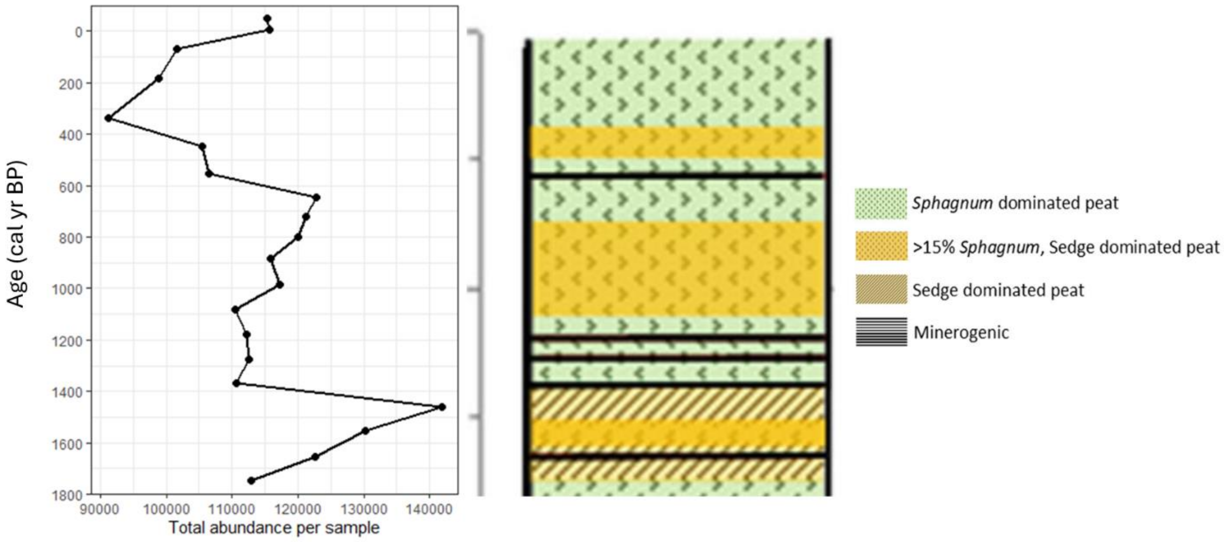

**Figure S10.** Total 16S sequenced abundance of bacterial phyla compared to the plant macrofossil record of Ryberg et al. 2022. Bacterial abundance is generally higher in sedge-dominated peat. The phase 400 – 500 yr BP is less obvious, which could plausibly reflect the growing importance of hydraulic conductivity in the upper few tens of centimetres in ombrotrophic peatlands.

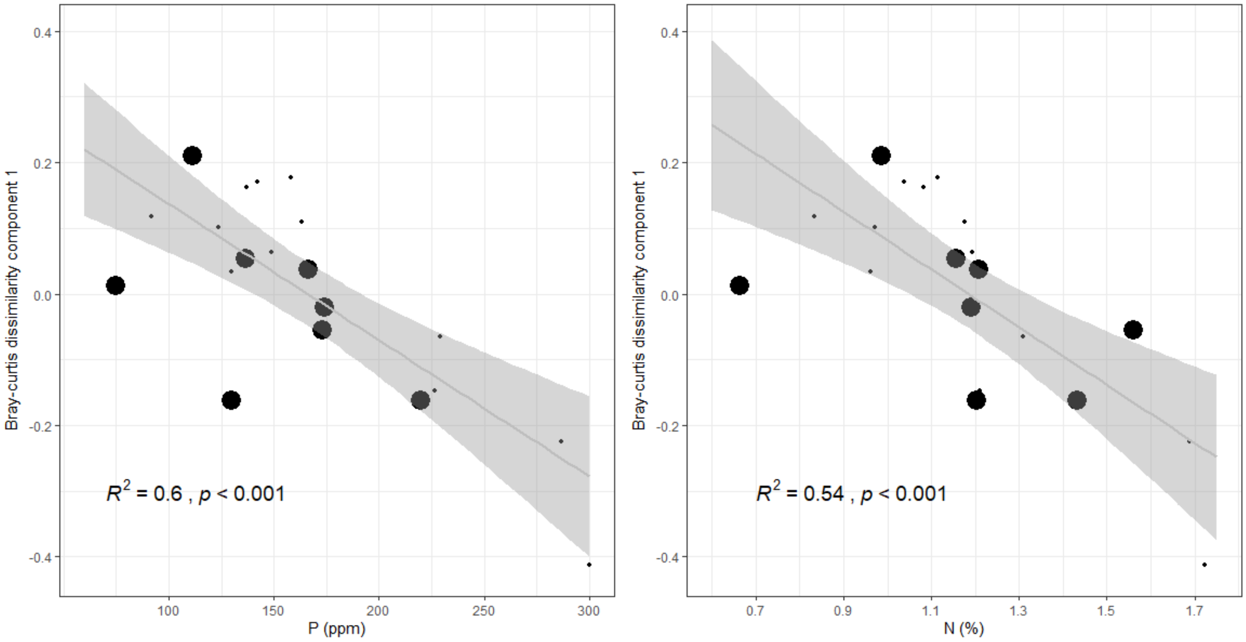

**Figure S11.** Scatter plots of nutrient concentrations against Bray-Curtis Component 1 score. Larger data points are the samples with high *Proteobacteria* abundance.

**Table S1.** End-member materials used in the NIRS end member multiple regression modelling (Russell et al. 2019).

| End-member name | Substance | Description |
|---|---|---|
| OHeather | Lignin | Woody, lignin-rich plants (powdered *Calluna vulgaris* stems, branches and leaves) |
| AvSHAFA | Humic/fulvic | Acid and alkali insoluble fraction from a basal organic rich peat sampled at Holcroft Moss. |
| OMMHumin | Humin | Acid and alkali insoluble fraction (HCl and NaOH) extracted from peat sampled at May Moss (Chiverrell 2001), which contains all degraded fine grained organic matter excluding plant materials and the alkali soluble humic/fulvic acids. |
| OSphag | *Sphagnum* | Bog mosses (powered *Sphagnum papillosum* capitulum, leaves and stems) |

**Table S2.** Main functional groups and associated wavelength regions from the FTIR-ANR analysis (Martínez Cortizas et al., 2024 and references therein).

| Region | Type of vibration |
|---|---|
| I: 3700-3000 | Vibrations corresponding to hydroxyl (O-H) from alcohols, phenols, carboxylic acids and polysaccharides. N-H vibrations from secondary and primary amides and/or C-H from alkynes. |
| II: 3000-2650 | C-H stretching vibrations of aromatics, alkanes, alkenes and aldehyde. |
| III: 1800-1650 | Carbonyl (C=O) bond vibrations in anhydrides, aldehydes, ketones, carboxylic acids, amines, oximes, and/or alkenes (C=C). |
| IV: 1650-1450 | Vibrations of N-H in primary and secondary amides, C=C in aromatics, C-H bending, and N=O. |
| V: 1450-1350 | Bondings and vibrations related to multiple chemical structures and functional groups, e.g. C-H and O-H deformations in phenolic and aliphatic groups. |
| VI: 1350-950 | Mostly associated with C-O stretching in polysaccharides groups in peat (1032 $cm^{-1}$), but may also contain vibrations related to (G and S) lignin structure. |
| VII: 950-700 | In peat, this region often represents C-H out of plane vibration in lignin and/or O-H stretching in polysaccharides. |
| VIII: 700-550 | C-O stretching in polysaccharides Si-O stretching in minerals. |